A V-shaped ultra-sensitive localized Surface Plasmon Resonance based Biochemical sensor

by

1.Rakib Hossain Antor (160021136)
2.Mahmudul Hassan Turja (160021146)
3.Ashikur Rahman (160021148)
4.Fahim Yasir (160021154)

A Thesis Submitted to the Academic Faculty in Partial Fulfillment of the Requirements for the Degree of

BACHELOR OF SCIENCE IN ELECTRICAL AND ELECTRONIC ENGINEERING

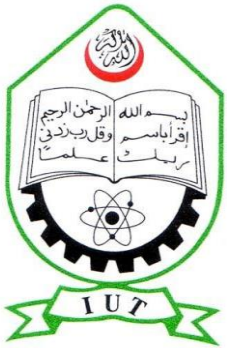

Department of Electrical and Electronic Engineering
Islamic University of Technology (IUT)
Gazipur, Bangladesh

March 2021

A V-shaped ultra-sensitive localized Surface Plasmon Resonance based Biochemical sensor

Approved by:

_____

Prof. Dr. Mohammad Rakibul Islam
Supervisor and Professor,
Department of Electrical and Electronic Engineering,
Islamic University of Technology (IUT)
Board bazar, Gazipur- 1704.
Date: ……

List of Contents

List of Tables

List of figures

List of Acronyms

PCF	Photonic Crystal Fiber
SPR	Surface Plasmon Resonance
SPW	Surface Plasmon Wave
SP	Surface Plasmon
SPP	Surface Plasmon Polariton
RIU	Refractive Index Unit
RI	Refractive Index
NIR	Near-infrared Region
EMI	Electromagnetic Interference
TIR	Total Internal Reflection
TE	Transverse Electric
TM	Transverse Magnetic
FEM	Finite Element Method
MM	Multipole Method
PML	Perfectly Matched Layer
PMC	Perfectly Magnetic Conductor
OFC	Optical Fiber Conference
PBG	Photonic Band Gap
HNL-PCF	Highly nonlinear PCF
IG-PCF	Index-Guiding Fibers

PBG-PCF	Photonic Bandgap Fibers Page
HA-PCF	Hole Assisted PCF
HC-PCF	Hollow Core PCF
HIC-PCF	High Index Contrast PCF
HNA	High Numerical Aperture
LMA	Larger Mode Area
AG	Air guiding
THz	Terahertz
SNR	Signal to noise ratio
LPG	Long period grating
FBG	Fiber Bragg grating
SERS	Surface Enhances Raman Scattering
AS	Amplitude Sensitivity
WS	Wavelength Sensitivity
LSPR	Localized Surface Plasmon Resonance
EML	Effective Material Loss
ITO	Indium Tin Oxide
TNT	Tri Nitro Toluene
CL	Confinement Loss
TC-PQF	Trapezoidal channel photonic quasi-crystal fiber
TiO_2	Titanium dioxide

Acknowledgement

All praise to the Almighty (SWT). By the grace of Him we were able with astounding results to complete our assigned thesis. Thank you, also, for your continuing support, supportive mood, good advice, polite manner and, most notably, your continuous persistence in the learning stages, our Thesis Supervisor Md. Rakibul Islam, professor, departmental professor of electrics and electronic technology, Islamic University of Technology. His helpful approach to us allowed us to work rapidly on our thesis and enabled us to complete the work in due course.

We would also like to thank all the Electrical and Electronics Department faculty for their helpful feedback and positive criticisms. During the research work, their supportive approach motivated us. Furthermore, this work of study will not have been done without our parent's constant love and motivation took our side whatever we tried to do. Last but not least, for all the seniors, juniors and well-wishers.

Abstract

PCF-SPR distinguishing joins the upsides of PCF development and plasmonic to decisively control the short-lived field and light expansion properties in single or multimode courses of action. In terms of SPR-based PCF sensor testing, several investigators have already shown excellence. They also suggested excellent designs with a high sensitivity to amplitude in recent years. The problem for design, though, is that most designs are sensitive to high losses or have low susceptibility and low losses. And the most critical thing is that the prototypes are dynamic to reach high sensitivity. In the simple design we were successful, we tried to eliminate these limitations and achieve great sensibility with a low loss. This research illustrates multiple parametric study based on surface plasmon resonance (SPR) of a slightly gold-coated photonic crystal fiber (PCF). In verifying sensing accuracy, the proposed sensors are not very sensitive to changes in structural parameters. Design and manufacturing error is restricted to a minimum. The sensor's prowess is investigated using the "finite element" approach (FEM). This paper demonstrated a theoretical study of a partially gold-coated photonic crystal fiber (PCF) based on surface plasmon resonance. In verifying sensing accuracy, the proposed sensor is not very sensitive to changes in structural parameters. Design and manufacturing error is restricted to a minimum. The prowess of the sensor is researched with the method “finite element” (FEM). The proposed model shows maximum wavelength sensitivity of 14000 nm/ RIU (Refractive Index Unit) with a sensor resolution of $7.14x10^{-6}$ RIU. Also, the maximum amplitude sensitivity is reported to be 4779.7 RIU^{-1}. The calculation is performed in the refractive index range of 1.33-1.41. The introduced device may be a better alternative for biosensors because of its simple structures, linear trait, and high sensibility.

Chapter 1

Introduction

1.1 Background

Surface plasmon resonance is a remarkable optical detection tool because of its extremely sensitive performance [1]. As light wave hits the metals sector, electrons at the metal-dielectric layer oscillate together. This is known as the surface plasmon wave (SPW). In the match between energy and dynamism of the light and SPW is a steep incline of reflected power. This is called the surface plasmon resonance (SPR) [2]. Due to its broad range of uses in environmental monitoring, medical diagnosis, biological analysis and chemical detection over the past few decades, SPR has become sufficiently familiar [3]. For its high sensing output, the Kretschmann SPR sensors are widely used, but they consist of moving mechanical components and are usually voluminous. At the time of miniaturization and improvement of these sensors, sensing applications became constrained. To eliminate these issues, optical fiber sensors are added [4]. Recently, photonic crystal fibers (PCF) provide a major role on sensor. PCF proved to be a successful substitute for prism. PCF is a promising candidate for SPR sensors by exploiting its advantages such as small scale, smoother start, single mode propagation and the potential to monitor evanescent field penetration. It is desirable to have a small physical configuration of the sensors. By the parameters such as pitch, number of rings, PCF air hole size, the sensitivity of the sensor is advanced [5].

The SPR occurrence is fabricated in most of the current PCF-based sensors using gold, silver, and aluminum. As silver does not have an inter - band shift and low damping loss, it can be seen as the exquisite plasmon, but it's sensing performance decreases when a delicate oxide layer is formed [6]. An additional plasmonic aluminum, though high electron density, is also affected by oxidation problems. Gold is, instead, an organic friendly alloy that is chemically stable under aqueous conditions. It also has high resonance peak changes and manufacturing viability [7]. In general, PCF-based sensors are divided into two categories. One is metal-coated sensors inside. Other sensors are externally painted metal. In a distinguishing air hole(s), all metal- and liquid analytes are mounted in the inner area of the PCF. In this segment, the first type of plasmonic material is

located. In the second model, the PCF external layer is accumulated by it [8]. Although highly sensitive, the plasmonic material in internal metal-coated sensors can't be deposited accurately within the labeled PCF region. In comparison, the plasmonic content and the analyte in externally metal-coated sensors are stored outside the plasmonic surface, making the manufacturing feasible and highly sensitive.

1.2 Motivation

Biosensor is an analytical instrument for the detection by sensing the refractive index of biological and biochemical analytes. For various refractive indexes the sensor exhibits various characteristics. The sensor sensitivity indicates that when the amount of the measurement is determined, the output of the sensor varies. Less sensitivity is the principal weakness on different sensors. This ensures that a transition is incredibly poor in wavelength. This response leads to changes in the analyte's refractive index (RI). The sensitivity of the sensor can be enhanced. The structural parameters of the PCF are optimized. Due to small changes in the analyte RI of PCF-based sensors indicate a high wavelength transition [2]. In addition to the use of chemically stable materials, broad resonance wavelength changes appear. Sharper resonance peak is required to detect accuracy [5]. Some SPR sensors based on PCF provide high sensitivity and great detection precision, but the structure is challenging for production. But it is necessary for a quick, successful design. A sensor is highly efficient, and can feel a wide range of RIs with simple design and high sensitivity.

1.3 Objectives of this thesis work

This study proposes several bio-sensors based on the PCF surface plasmon resonance (SPR). The main aims of the study are:

- To carry out a comprehensive literature analysis of SPR sensors
- Extending the dynamic sample analysis detection range.
- Utilization of gold outside of the PCF framework makes the manufacturing process acceptable.

- The veracity of the sensor is examined across various evaluation parameters.
- Identification of biological analyses for outstanding responsiveness, greater resolution and adequate linearity.

1.4 Expected outcomes

- Some SPR based sensors are designed for determining uncertain analytes.
- These proposed designs will monitor a diverse range of refractive indices.
- Gold is used exogenously as plasmonic material for practical production.
- The optimum specification parameters that are deliberately chosen will have better resolution.
- An increased susceptibility can be achieved, which ensures that the design parameters of the proposed sensor are effectively investigated.

1.5 Methodology

This chapter uses all of the mentioned numerical tools and methods correctly to build a basic, highly sensitive bio sensor. These techniques and the computational instruments are needed to achieve likely results and meet the expectations.

1.5.1 Finite Element Method

The Finite Element (FEM) approach is a computational way to solve the engineering and mathematical physics problems. The mathematical problem's empirical approach usually requires the solution to boundary value problems for partial differential equations. The problems are formulated and an algebraic system is developed. The approach is based on the unknown domain function [10]. In order to solve this problem, a complex structure is divided into smaller, simple pieces called finite elements. The basic equation of the modeling of these finite elements is then

put together in a broader equation framework that represents the whole problem. FEM then uses different approaches to approach the solution by decreasing the resulting error function from calculating the variables.

A general procedure for finite element analysis:

1. Pre-processing: Defines the problem's geometric domain. – Specify the type(s) of element to use. – Defining elements' material characteristics. – Defines the elements' geometric properties (length, area, and the like). – Identify networking feature (mesh the model). – Set physical limitations – (boundary conditions). Define loadings. Define loadings. The calculated values are then used by backup to quantify extra, deducted variables such as reaction forces, factor stresses and thermal flow by calculating the unheard-of values for the primary field variable(s).

2. Post-processing: Postprocessor's platform includes advanced routines for chosen data from a final element solution used for processing, printing and tracking.

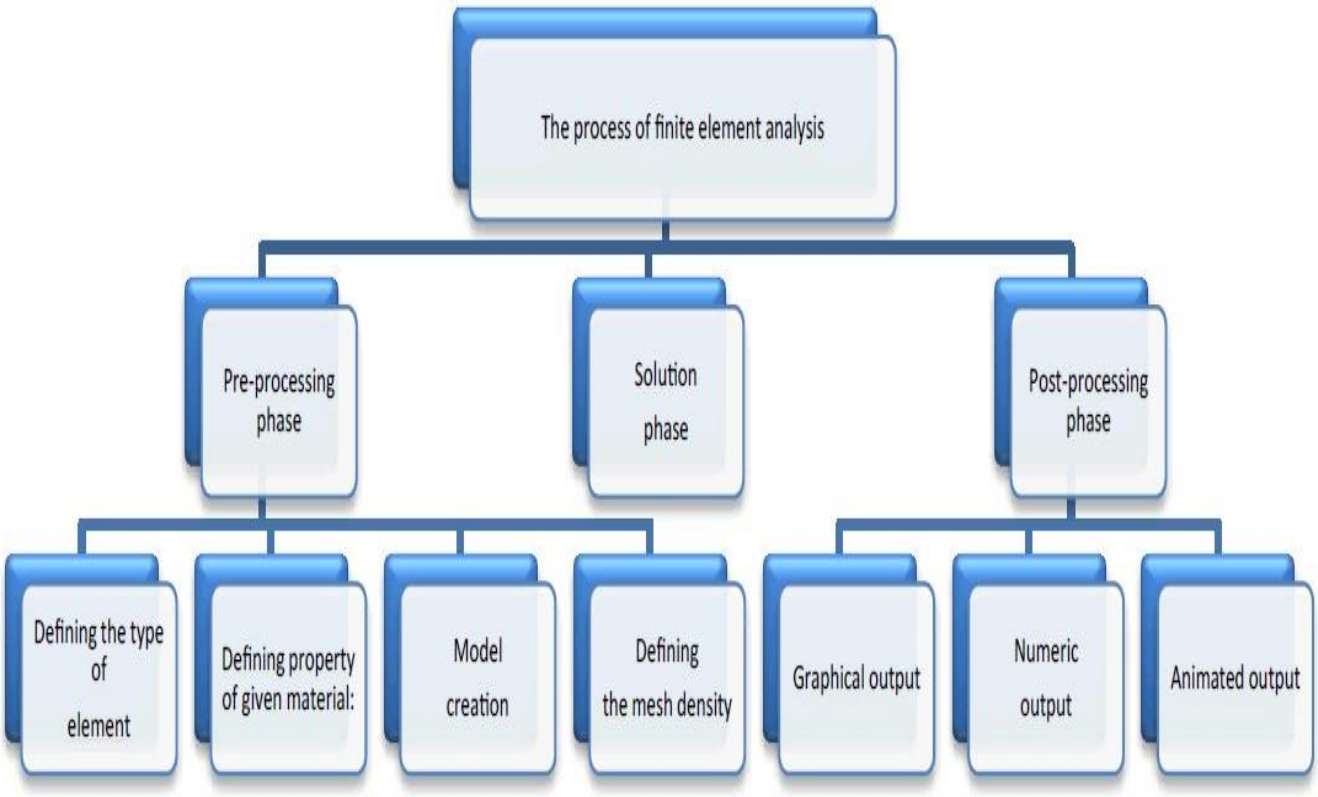

Figure 1.1: The Process of Finite Element Analysis

1.5.2 Perfectly Matched Layer (PML)

The perfectly matched (PML) layer for wave equations is a manmade absorption surface widely used in numeric methods for truncating computational regions in order to simulate open boundary problems. The primary property of a PML that makes it different from a normal absorbent material is that it has been engineered to prevent waves occurring on the PML from reflecting on a non-PML medium at the interface – this property enables the PML to take off waves powerfully from within the computer region without reflecting them within.

PML was first proposed by Berenger in 1994 for use with Maxwell equations, and since then there have been many similar PML reformulations for both Maxwell equations and for other wave-type equations, such as electrodynamics, linear Euler equations, Helmholtz equations, and photoelasticity. Initial Berengers formulation is known since PML, as it separates the electric fields into the PML region into two non-physical fields. A late, more common formulation is known as uniaxial PML (UPML) or artificial anisotropic material which, because of its simplicity and quality, has been identified [11-13].

1.5.3 Numerical methods and sensor designing

1.5.3.1 Effective Refractive Index

The refraction index is the metric by which radiation speed and wavelength in relation to its vacuum value are decreased. The speed of light in a medium is $v = c/n$, and similarly the wavelength in that medium is $\lambda = \lambda 0/n$, where $\lambda 0$ is the wavelength of that light in vacuum.

We have modified the effective layer refractory index for optimal resolution and sensitivity in this document.

1.5.3.2 Confinement loss

Containment losses are the losses due to the mode's faulty condition and the non-perfect PCF fiber structure. Then modes are driven with a structure-dependent loss relying on the wavelength, frequency of hole rings, and hole size.

The dynamic RI of fundamental mode can be resolved by using Maxwell's equations as its own eigen value problem with the FEM [14]. Such loss is determined by core size, pitch and air-holes, number of cladding rings, etc. We must use a highly sensitive SPR sensor for low loss.

1.5.3.3 Wavelength interrogation method

The SPR sensitivity depends on the maximum wavelength resonance transition. The wavelength interrogation process can be used for evaluating. This approach has multiple benefits over the identification of amplitude method. It offers increased sensitivity, stability and versatility. Sensitivity here is defined as [15]

1.5.3.4 Amplitude interrogation method

The sensitivity of amplitude does not require interpolation of the wavelength and is thus easy and cost effective. [16]

1.5.4 Software used in this thesis work

We have used three software primarily to perform the thesis. They are explained as follows:

1. COMSOL Multiphysics: Multiphysics software is designed from the ground up to be able to integrate models of various phenomenon of physics in any manner they choose. Multiphysics software Perhaps this can be done easily by using the software's built-in functions, but in most situations the user has something additional to do. With this, we can conveniently define subdomains and boundary conditions with the right parameters and solve problems for both

electrical fields and magnetic fields, designing Photonic Crystal Fiber. COMSOL Multiphysics 5.3.a is used to prototype the arrangement**.**

2. MATLAB: In this wok, MATLAB is predominantly used to obtain the limit loss curve, resolution curve, wavelength-sensitivity and amplitude-based responsiveness

3. Microsoft Excel: The information gathered by COMSOL program 5.3.a was stored and then sent to MATLAB to receive the desired different curves mentioned in the last segment.

1.6 Thesis framework

Chapters are used in the thesis. This shows the entire work to achieve the targets and likely results mentioned in previous pages.

Chapter 1: Discuss the context and goals of this study of SPR-based PCF biosensors. It also outlines the potential planned results and methods of this study

Chapter 2: Discuss the basic introduction optical fiber communication, different types of optical fiber, basic steps and application.

Chapter 3: Presents the background history of optical bio sensor and literature review.

Chapter 4: Based on basic idea, history, classification, mechanism of photonic crystal fiber.

Chapter 5: Explains the basic principle and sensing mechanism of surface plasmon resonance and also its advantages and applications.

Chapter 6: It consists of introduction, brief sensing mechanism of PCF based SPR sensor, and also the advantages of using it over prism-based sensor are also discussed

Chapter 7: Consists of the structure, design of the proposed PCF based SPR sensor. The performance parameters are studied and results, graphs are also showed in this chapter

Chapter 8: It is mainly the conclusion of the whole work. Limitations and some recommendations are also prescribed here.

1.7 Summary

This chapter has enclosed the information about the research. Both the aims, methods, predicted results and potential analyzes of the work are momentarily addressed here so that the basic concepts and outline of the study are conveniently obtained. The objective and likely achievements of the thesis work are also reflected.

This chapter has presented the succinct nature of the study. The research's priorities and aims were also outlined, which provide a clear picture of the whole study.

Chapter 2

Background and literature review

2.1 Background

Since last few decades, optical biosensors are widely used to monitor and analyze the molecular interactions. Optical sensors have gained enormous attention for its easy instant detection capability due to advance optical instrumentations. In the late 1980s, first optical biosensor had been commercialized. The fundamental theory behind any optical sensor is related to light issues where light intensity or electromagnetic fields change due to the presence of samples. A specialized instrument that is capable of converting light rays into electrical signals and can also be used to track changes and reactions in the atmospheric condition or to determine the strength of electromagnetic waves called optical waves.

Wood first clarified the understandable facts of the SPR in 1902. In the mirrored sun, he found a kind of "exceptional" divergent. As the polarized light blew on a glass with a scattering grating. Subsequently, instead of attempting to explain this interesting phenomena for decades, an extensive explanation of the SPR could not be given until 1968.

In 1993, R.C. Jorgenson first introduced optical fiber based on the SPR sensor, where the gold film was used in the fiber core to expose the PCF response to plasmon because it has different attractive characteristics, e.g. controllable birefringence, high containment and single-mode propagation. Using these characteristics, the evanescent field can be easily manipulated. The efficient and responsive output of the fiber is influenced by the evanescent field.

In 1983, Liedberg et al. first showed the use of an SPR-based sensor to detect biomolecular interaction. They were able to understand the direct and immediate identification of biomolecular activity by applying the SPR sensing tool. SPR sensor technology has been gaining huge interest as well as continually evolving since then. The first commercial SPR biosensor started in 1990 on the basis of the Kretschmann configuration called the Biacore instrument. The third era of fiber optic communication working at a wavelength of 1.55 μm was created in 1990. The fourth era of fiber optic frameworks utilized optical speakers as a trade for repeaters, and used wavelength

division multiplexing (WDM) to build information rates. The fifth era fiber optic communication frameworks utilize the Dense Wave Division Multiplexing (DWDM) to additionally expand information rates.

Nowadays, SPR sensors offer high sensitivity rather than fiber-based sensors. It also offers a low resonance peak than a fiber-based sensor. The PCF-based sensors also have a modular interface. Most PCF-based SPR sensors use gold or silver. Here, in this elevated structure, we assume the gold layer since the gold is chemically stable and exhibits greater changes in wavelengths of resonance.

2.2 Literature review

Various types of plasmonic materials such as gold, copper, silver and aluminum plasmonic materials are used in PCF-based SPR sensors [17]. This plasmonic materials may be placed either externally or internally. Many prior works with different designs of different plasmonic content have been studied. The PCF is internally coated in [18]. Thin gold and TiO_2 film are mounted on the surface of the air holes. The phase-matching state of the plasma and fiber modes is ultra-sensitive to the refractive index (RI). This property has created considerable interest in the exploration of plasmon fiber designs for RI sensing applications. A significant parameter, i.e. the containment loss associated with the imaginary part of the effective mode index of the fiber waveguide mode, is typically used to characterize the plasma sensor, in particular the amplitude investigation and wavelength investigation methods.

A PCF SPR sensor with larger biosensor outlets has been proposed. This PCF has a wavelength sensitivity of 2000 nm/RIU. Amplitude sensitivity of 300 RIU^{-1} occurs at refractive indices from 1.33 to 1.39[19]. These are achieved with a resolution of 2.5×10^{-5} and 2.1×10^{-5} RIU, respectively, at refractive indices between 1.33 and 1.37. Another D-Shaped PCF dependent graph is a wavelength sensitivity of 3700 nm/RIU. It has a resolution of 2.7×10^{-5} RIU in [2]. A DS formed PCF modeled in [49]. It given an average and maximum sensitivity of 7700 and 9000 nm/RIU. Two externally gold-coated hexagonal photonic crystal fibers (H-PCFs) are also investigated in [9]. Paper [9] shows a wavelength sensitivity of 4000 nm/RIU and amplitude sensitivity of 478 RIU^{-1}. These are achieved with a resolution of 2.5×10^{-5} and 2.1×10^{-5} RIU,

respectively, at refractive indices between 1.33 and 1.37. In [20] wavelength sensitivity of 4000 nm/RIU with amplitude sensitivity of 320 RIU^{-1}, sensor resolutions of 2.5 × 10−5 and 3.125 × 10^{-5} RIU at sensing range of 1.34 to 1.36 are achieved. A multi-channel PCF-based sensor using plasmonic silver material coated with gold has been presented in [89]. It shows wavelength and amplitude sensitivity of 4750 nm/RIU 1555 RIU^{-1} [89]. A D shaped hollow-core PCF sensor has a wavelength and amplitude sensitivity of 6000 nm/RIU and 148 RIU^{-1} [90]. Various types of sensors of varying wavelength and amplitude sensitivity are observed from the above sample. They all have different structure. Problem claims are certain sensors with low sensitivity and some with difficult designs. For a good sensor, high sensitivity and fine resolution are desirable. And from the other hand, the scale of practical manufacturing is important for the design. Some of the proposed designs placed plasmonic material in inner air holes that are difficult to manufacture. The previous study showed the potential for spiral manufacturing as well as the external surface covering of the material.

This paper discusses a simple PCF based bio sensor to achieve high sensitivity. A coating of gold is used as a plasmonic substance on the outer surface of the PCF structure. This is done to improve the identification and manufacturing process. Sensitivity of the wavelength, sensitivity of the amplitude, resolution of the sensor and linearity are primarily used. These are numerically examined in the refractive analyte index between 1.33 and 1.40. In order to achieve optimum sensing accuracy, the design parameters are studied here. These include pitch, air hole diameter and the thickness of the gold sheet.

Chapter 3

Optical fiber communication

3.1 Optical fiber

An optical fiber cable is an arrangement similar to an electrical cable, but containing one or more optical fibers used to carry light. The optical fiber components are usually individually coated with plastic layers and are enclosed in a protective tube appropriate for the setting in which the cable is used.

3.2 Optical fiber waveguide

A circular dielectric waveguide or fiber optic has an internal center that has a higher refractive index than the cladding. There is an angle at a certain diameter which is less than the critical angle so that there is a complete internal reflection.

3.3 Transmission through fiber

Fiber optical communication frameworks consist of an optical transmitter to turn over an electrical signal to an optical signal for transmission via an optical fiber, a link comprising a few groups of optical filaments, optical enhancers to help the optical signal strength, and an optical receiver to convert the received optical signal back to the first transmitted electrical signal.

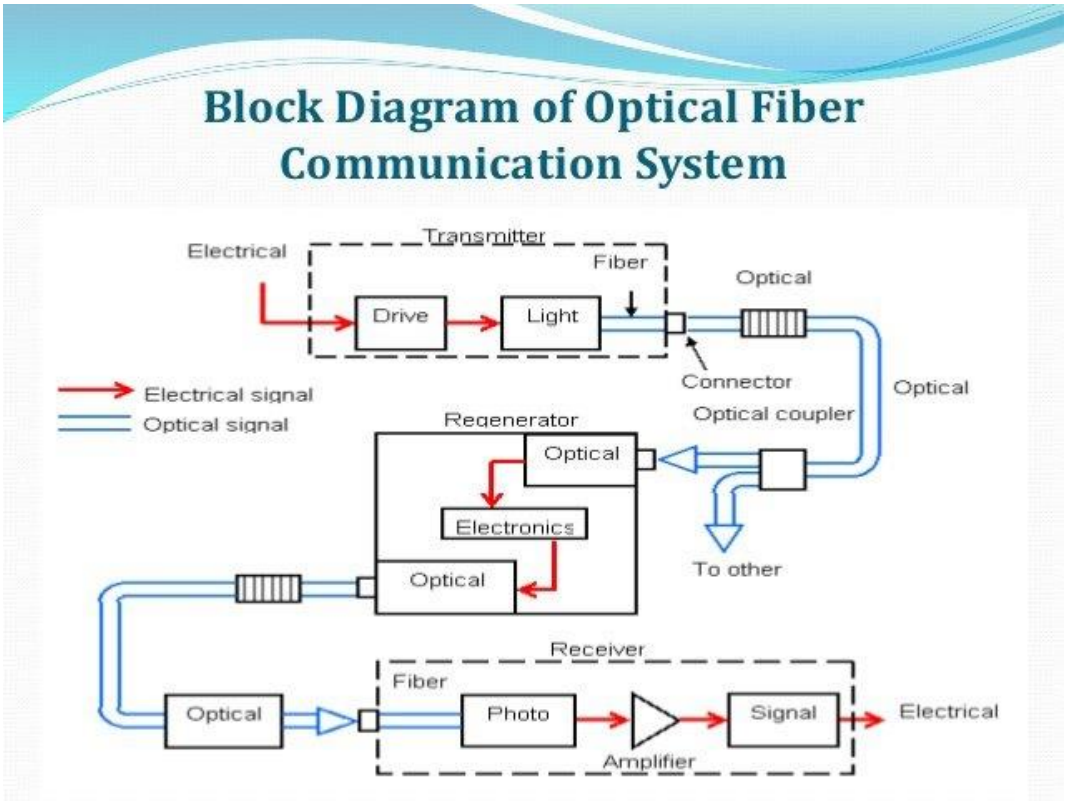

Figure 3.1: Basic optical fiber communication block diagram.

3.4 Types of optical fiber

Optical fibers fall into two major types:

- Step index optical fiber
- Graded index optical fiber

3.4.1 Step Index Optical Fiber

Step Index of optical fiber, which incorporates single-mode optical fiber and multimode optical fiber, and checked record optical fiber. Single phase fiber optic file has a center width of less than

10 microns and allows only one light path. Multimode phase index optical fiber has a center14 measurement that is more noteworthy than or equal to 50 micrometers and allows for a few light paths, resulting in modular dispersion.

3.4.2 Graded Index Optical Fiber

Graded index optical fibers have their center refractive record decrease bit by bit more distant from the focal point of the center, this expanded refraction at the center of the center reduces the speed of certain light beams, thereby allowing all light beams to reach the receiver at about the same time, along those lines, which reduces the dispersion.

3.5 Birefringence

Birefringence is the optical property of a material with a refractive index that depends on the direction of polarization and light propagation. These optically anisotropic materials are said to be. Birefringence is often quantified as the maximum difference between the refractive indices shown in the material.

3.6 Application

Optical fiber is used by a number of broadcast service companies for the transmission of telephone signals, Internet communication and satellite TV signals. Because of much lower constriction and impedance, optical fiber has tremendous interest in long-separation and appeal applications over existing copper wire. However, framework advancement within urban areas was typically difficult and time-consuming, and fiber-optic frameworks were thought-provoking and expensive to implement and operate.

Chapter 4

Photonic Crystal Fiber

4.1 PCF in brief

Photonic-crystal fiber (PCF) is one kind of optical fiber, which is based on the characteristics of photonic crystals. PCF is finding applications in fiber-optic interchanges, fiber lasers, nonlinear devices, and high-control communication due to its ability to block light in empty centers or with constraint properties that are impractical in ordinary optical fiber. Photonic crystal fibers are a subset of a larger category of microstructure optical fibers, in which light is driven by structural changes rather than refractive index variations.

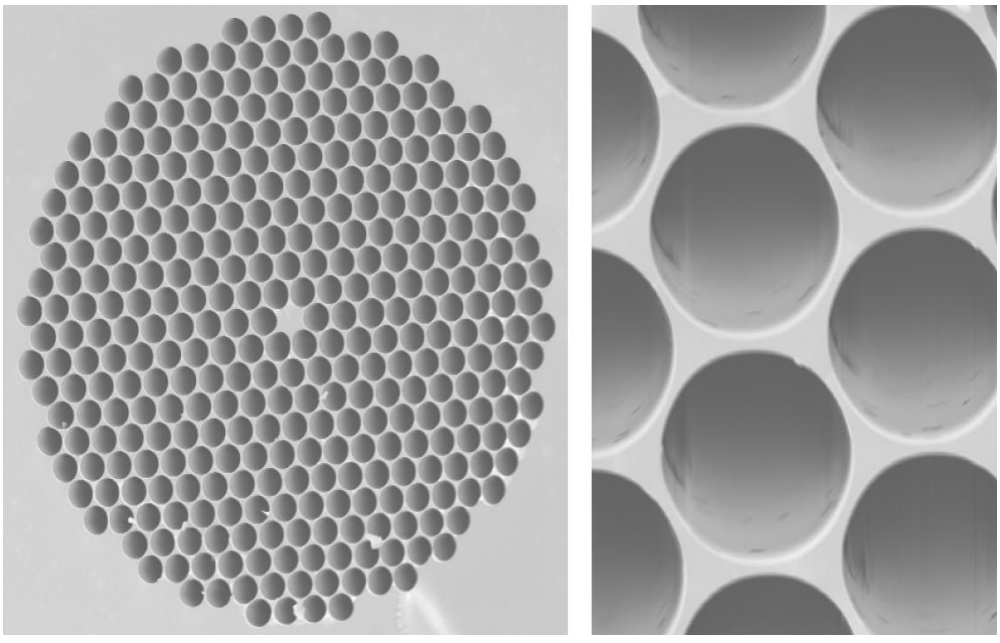

Figure 4.1: Photonic Crystal Fiber (PCF)

4.2 Classifications of PCF

Classifications of PCF depends on structures. Based on this Index-Guiding Fibers (IG-PCF) and Photonic Band-gap Fibers (PBF) are the two major types of PCFs (PBG-PCF).

Highly Nonlinear Fibers or HNL fibers, Mode Area fibers (LMA fibers) and High Numerical Aperture fibers (HNA fibers) are examples of Index Guiding PCFs or IG-PCFs. HNL fibers have a limited core dimension to ensure close mode isolation, HNA fibers have a microstructure cladding with a ring of air holes surrounding the cladding, and LMA fibers have a larger core dimension and a low refractive index to ensure a larger effective field.

Air-Guiding fibers (AG fibers) or Hollow Core (HC fibers) and LIC fibers or Bragg fibers are two types of Photonic Band-gap Fibers (PBG-PCFs).

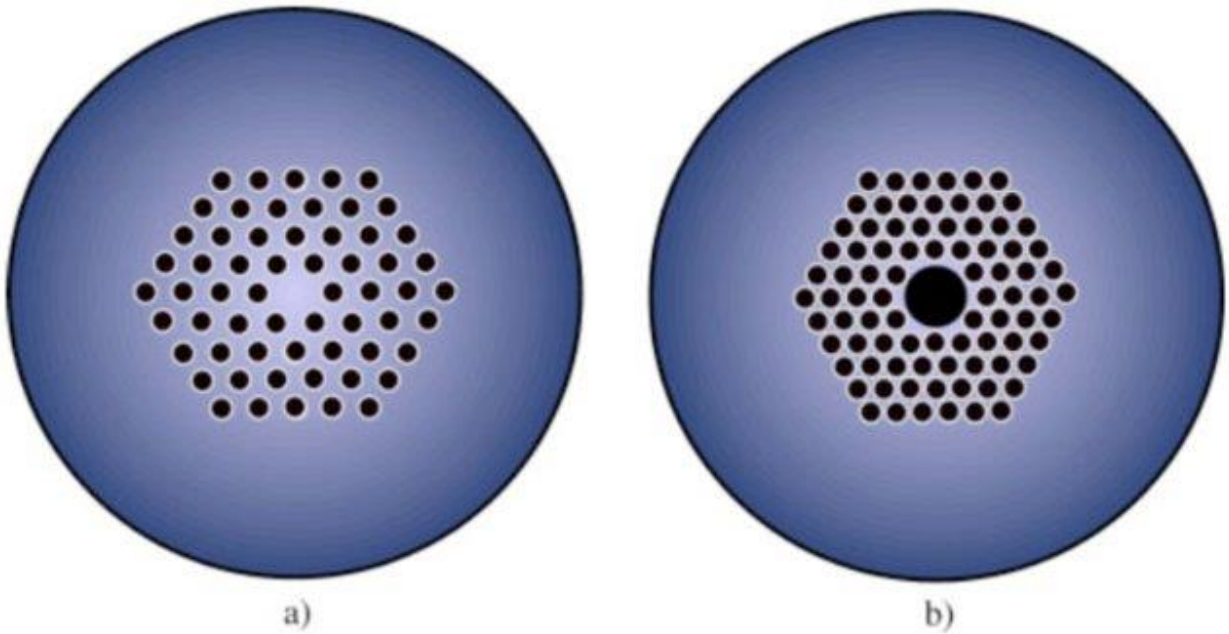

Figure 4.2: (a) Index-Guiding PCF; b) Photonic Band-gap PCF.

4.3 Construction of PCF

Usually, such fibers are created using methods that are similar to those used to make other optical fibers: first, a "preform" the size of centimeters is formed, and then the preform is warmed and drawn down to a much smaller distance across, contracting the preform cross region while maintaining similar highlights. A single preform can be used to make kilometers of fiber in this manner. Stacking is the most well-known method, including the fact that boring/processing was used to deliver the key aperiodic structures. The key fragile glass and polymer structured strands were created as a result of this. The majority of photonic gem fibers are made of silica glass, although some glasses have been used to achieve complex optical properties. There's also a growing interest in manufacturing them out of polymer, with a variety of structures being studied, such as checked list structures and ring ordered fibers MPOF stands for small scale structured polymer optical strands and is the name given to these polymer fibers. Temelkuran et al. (2002) used a polymer and chalcogenide glass combination for 10.6 m wavelengths where silica isn't readily available.

4.4 History of PCF

In 1978, Yeh et al. [22] introduced the idea of a PCF for the first time. He proposed cladding a fiber core with Bragg grating. This is similar to a one-dimensional photonic crystal. In 1992, P. Russell developed a PCF containing a 2D photonic crystal with an air nucleus. In 1996, the first PCF was unveiled at the Optical Fiber Conference (OFC). In the year 2000, eminently birefringent PCF was introduced, and for the first time, super-continuum technology with PCF was discussed [21]. The first time a Bragg fiber was formed was in 2001. For the first time in that year, a PCF laser with a double cladding was also shipped [14]. PCF with ultra-flattened dispersion was introduced in 2002. In 2005, researchers promoted large power transfer, low-loss alterations among PCFs, and photonic band gaps at 1% index comparison. In 2008, the polarization dependence of stimulated Brillouin spattering in small-core PCFs was discovered for the first time. After that, in 2009, nonlinear inter-core coupling in triple-core PCFs was implemented [22]. Then,

in 2010, devolving four wave mixtures were used to establish Diffraction and nonlinear coefficients for PCF. For the first time in 2011, an elliptical cone porous-core PC-PBGF was available.

4.5 Distinction between PCF based fiber and Traditional Fiber

The core of a traditional optical fiber has a higher refractive index than the cladding. The central area of a high RI material is doped to make it have a RI greater than the silica cladding. Germanium is commonly used to increase the refractive index of the nucleus, while fluorine is commonly used to decrease it. PCF, on the other hand, is composed of a single substance with very small air gaps embedded in a silica background. The index contrast between the center and the cladding is quite low in traditional fibers, but it is very strong and stable in PCF. This is accomplished by analyzing the variation in optical properties of two fibers [23]. PCF exhibits very low or very high nonlinear effects, broader single mode action, strong birefringence, smooth dispersion, and many other characteristics [24].

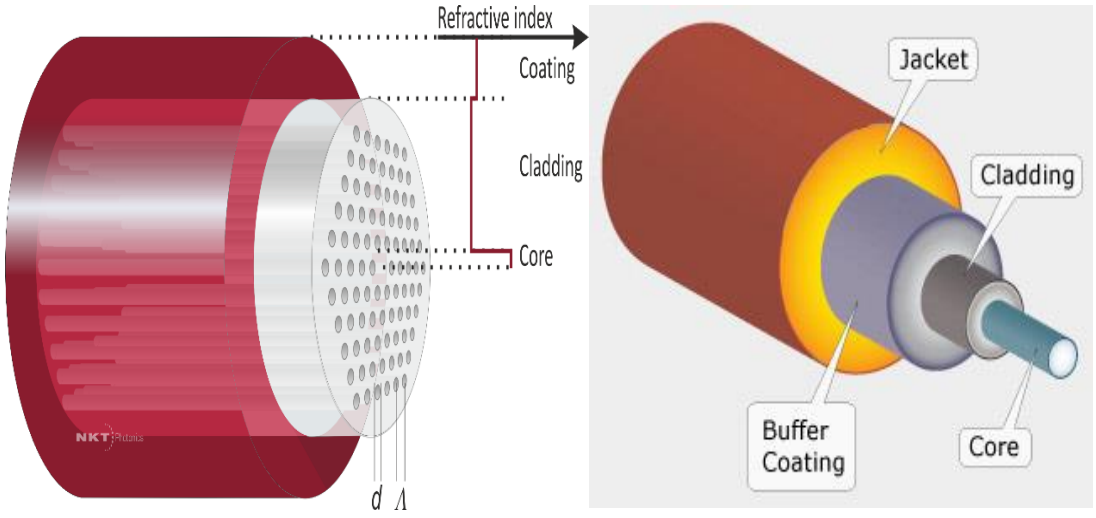

Figure 4.3: Cross sections and index-profiles of (a) PCFs and (b) Ordinary fibers

4.6 Light guiding mechanism of PCF

The most fundamental and well-known theory of guiding light in traditional fibers is Total Internal Reflection (TIR). A solid center is surrounded by a covering with a standard periodic series of air holes in the majority of TIR crystal fibers [25]. PCFs are a type of optical fiber with a periodic array of micro capillaries which create the cladding across a firm or void defect core [26]. The design of the PCF geometry, together with the wide range of materials available for manufacturing, allows for a wide range of optical properties to be tailored, including modal field, chromatic dispersion, nonlinear effects, and birefringence. PCFs can outperform their traditional counterparts in a wide variety of applications, including large-mode area infinitely single-mode fibers, dispersion adjustment, single-polarization and high birefringence regulation, and nonlinear applications.

4.7 Properties of Optical Transmission Fiber

Structural properties of optical transmission fiber include EML, confinement loss, birefringence, bending loss, chromatic dispersion and effective area which are discussed in the following sections:

4.7.1 Effective Material Loss

The critical parameter to consider for long-haul transmission in an optical fiber is efficient material loss (EML). Because of EML, signals are continuously dropped and cannot fly a long way. The EML is a measurement of the overall amount of light energy consumed by the core element.EML decreases as core voids increases so there are less components within the core, resulting in less absorption loss. As core diameter expands, EML expands as well. Also, since the lower frequency light wave travels through the air vents of the cladding field, EML rises as frequency increases [27].

4.7.2 Confinement Loss

The containment failure of a THz PCF is an important guiding property since it determines how long the actual THz transmission mechanism can last. The lack of air holes in the middle locale causes optical mode leakage from the inner center field to the outer air gaps, resulting in containment failure [28]. It's defined as the reduction caused by the standard cladding's finite magnitude [29]. The sum of air holes, the depth of the air hole, the number of layers, and the pitch will all affect confinement failure. Since a high frequency range and small core permeability result in more intense light in the core, confinement loss is inversely proportional to frequency. Confinement loss decreases as the core diameter increases, but increases as the permeability grows. In comparison, as core permeability rises, the index gap falls, allowing light to steadily disperse to the cladding area and thereby increasing confinement loss [30].

4.7.3 Birefringence

In fiber optics, and many other areas where birefringence is used to sustain light in a linear polarization state, birefringence is a valuable property. This optical effect is most often seen in materials with uniaxial anisotropy, which occurs when a material's optical axis has no associated axis in the direction perpendicular to it. Linearly polarized light waves in parallel and perpendicular directions would have varying refractive indices, ne and no, respectively, for irregular light rays. As a non-polarized beam of light passes through fabric at an extreme non-zero angle to the optical axis, the perpendicularly polarized portion can exhibit refraction at a regular angle and its reverse part at a slightly different angle, as shown by the difference between the two effective refractive indices known as the birefringence amplitude [30]. Since the index distinction between orthogonal polarization modes rises as frequency increases, birefringence strengthens. It's also worth noting that the magnitude of birefringence decreases as porosity increases, so increased porosity causes more strength to spread beyond the core zone, lowering the index distinction between polarization modes [31].

4.7.4 Bending Loss

For the functional application of a THz waveguide, bending loss is a critical parameter. Bending loss reduces as frequency increases. Since the fiber does not absorb sufficiently light within the center as the index contrast is even further reduced by the vulnerable air holes in the fabric, it is strong for large values of porosity and smaller bending radii [28]. Furthermore, bent loss is insignificant in comparison to other losses.

4.7.5 Chromatic Dispersion

Pulse expansion causes chromatic dispersion, which is one of the most common issues in fiber optic communication systems. Dispersion may occur in the material or in the waveguide [29]. However, since the substance has a constant RI within the frequency range under consideration, the substance dispersion can be overlooked since light dispersion in the sample is insignificantly low. High waveguide dispersion can reduce bit error rates during transmission, but it should be kept low for efficient transmission [30]. Pitch and radius changes affect the effective refractive index, causing dispersion to change. When a greater pitch value is used, dispersion increases, whereas when a smaller pitch value is used, dispersion decreases [32]. It's also worth noting that as frequency rises, dispersion decreases [33]. High dispersion slows down data processing and makes it less reliable, so it's a problem that needs to be addressed.

4.7.6 Effective Area

A main property of PCF is its efficient modal region. PC-PCFs with a large effective modal region are needed for communication and other elevated applications. The effective modal area is used to calculate the total area where the basic mode is active. As the mode increasingly expands with increasing frequency into the cladding zone, the effective area decreases, reducing the area of the fiber inhabited by the simple mode [30].

Chapter 5

Surface Plasmon Resonance

5.1 Surface Plasmon

There are a number of free electrons inside a conductor (metal), and an electron assembly can be viewed as a plasma particle. Simultaneously there are equivalent numbers of positive charged particles from grid so the all-out charge density in the conductor is zero. Now, once an external field is applied, the electrons will travel to the positive area and the positive ion will move as opposed to the electrons at the same time. Plasmon oscillation in the metal longitudinal oscillation will be added in the conductor because of this movement process, and this is known as the plasma oscillation known as surface plasmons.

5.2 Surface Plasmon Wave

A glass substrate with a thin gold coating is used to create SPR sensors. The light travels through the layer and from the gold coating is reflected. A part of this light energy produce resonant oscillation of the conduction electron at some angles of incidence through the gold coating, resulting in a surface plasmon wave at the sample and gold surface interface.

The incidence angle needed to preserve the surface plasmon wave is extremely sensitive to changes in refractive index at the surface as well as the thickness of the sample and gold layers due to mass change. It is these shifts which are used to track biomolecules' connection and dissociation. So, surface plasmon wave is the main factor for surface plasmon resonance.

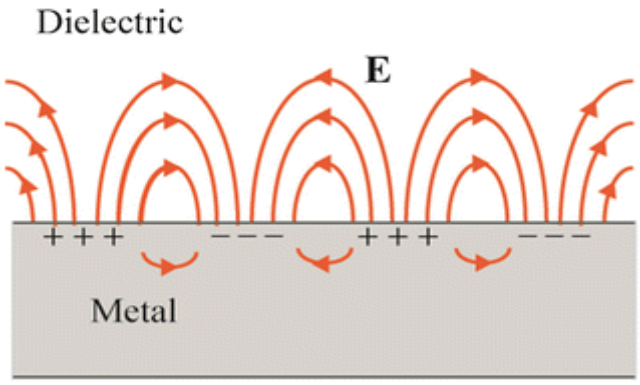

Figure 5.1: Surface Plasmon Wave propagation

5.3 Evanescent Field

A large amount of the strength is reflected into the cladding or medium that surrounds the center as light reflects at angles above the critical angle. The evanescent wave is a phenomenon that only lasts a small distance from the interface, with power decreasing exponentially as distance increases. . The evanescent field has been used to investigate surface-specific detection activities in real time. While absolute internal reflection is commonly used in optical fibers to guide light energy down the fiber, a section of the internally reflected wave travels a limited distance beyond the core edge and then into the optical cladding. This evanescent wave property can be manipulated by eliminating the fiber cladding, allowing the evanescent wave to spread past the core boundary into substances surrounding the fiber core. The intense evanescent electric field in a device with an absorbing dielectric medium enhances the medium's absorption [34].

5.4 SPR basis

Surface plasmon resonance (SPR) is the excitation of electromagnetic waves known as surface plasmon waves (SPW), which propagates through the boundary between a metal and a dielectric medium. The evanescent wave will excite the surface plasmon. The amplitude of the reflected light

sharply decreases as this occurs. The excited surface plasmons decays provide energy transfer to photons [35]. The reciprocal association of evanescent field and surface electrons is the basic operating mechanism of PCF-based SPR sensors. The evanescent field directs the molecules' binding, resulting in the SPW. This phenomenon, in short, causes SPW to interfere with the sensing substrate. The geometrical parameters of the PCF determine the accuracy of the SPR sensors.

5.5 Localized Surface Plasmon Resonance

Collective electron charge oscillations in metallic nanoparticles that are excited by light are LSPRs (localized surface plasmon resonances). At the resonance wavelength, they demonstrate higher near-field amplitude. This field is extremely localized at the nanoparticle and quickly decays into the dielectric environment away from the nanoparticle or dielectric interface, however the resonance often strengthens far-field dispersion by the molecule. Enhancement of light intensity is a very significant feature of LSPRs and localization ensures that the LSPR has a very large spatial resolution, restricted only by the size of nanoparticles. Due to increased field amplitude, LSPRs often improve effects that depend on the amplitude, such as the magneto-optical effect [36].

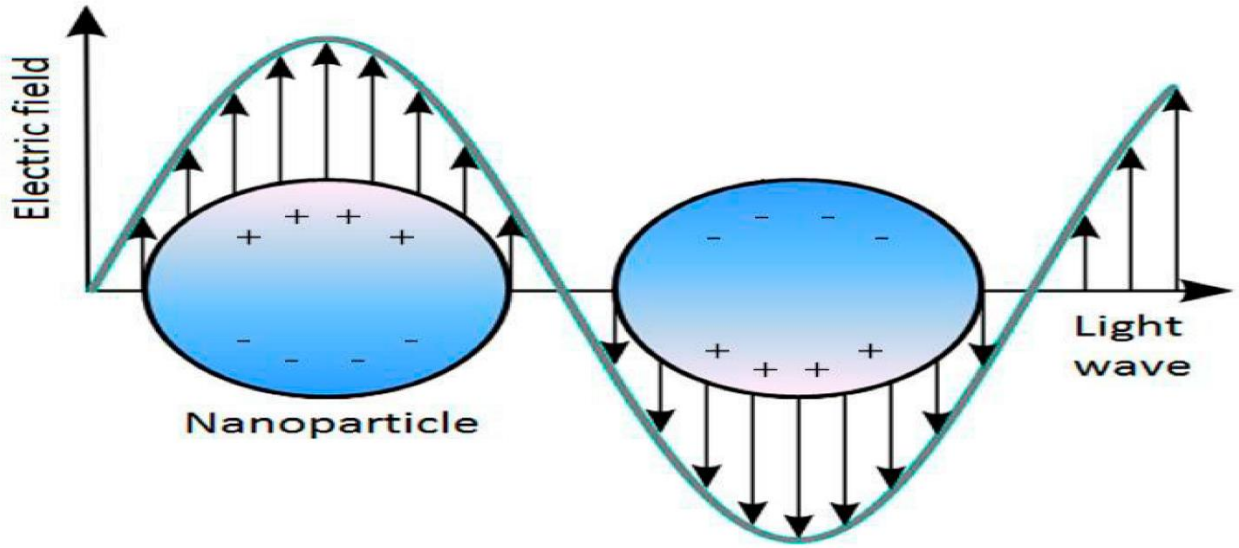

Figure 5.2: Illustration of the Localized Surface Plasmon on the surface of a nanoparticle [37]

5.6 Research motive of working with SPR

Because of its persistent, name-free, and noninvasive existence, surface Plasmon resonance (SPR) has been a major optical bio sensing breakthrough in the zones of natural chemistry, research, medicinal sciences and medical diagnosis after its first use in a continuous analysis of an organic structure in the 1990s. Business SPR devices are prohibitively expensive and involve consumable sensor chips that suit specific applications. Because of the high operating costs, this approach is expected to be taught in research center classes at the undergraduate level. Furthermore, the company SPR instrument is not a good demonstration device since all of the equipment pieces are encased, prohibiting understudies from imagining the SPR instrumentation's subtleties.

Food quality, hygiene, medical research, bimolecular analyte identification, and medical diagnostics are all potential applications for SPR technology [3]. SPR modes sponsored by PCF have gotten a lot of attention in recent years because of its ability to change optical parameters by design via the structure's configuration, (ii) light weight and (iii) easily controlled birefringence, making it a good choice for variety of sensing applications [38-42].

5.7 Excitation of SPR

An incident light beam may be used to excite surface Plasmons in a resonant way. Normally, visible and infrared light are used. The incoming beam must have the same velocity as the Plasmon. There are two possibly the best configurations for using light to excite SP waves.

Otto-configuration

Otto configuration was released in 1968. It is an ATR technique that is used to stimulate SPR. It's done by combining evanescent wave (EW) and surface potential wave (SPW). This is the concept behind this setup. Prism reliant architecture is used at the metal-dielectric interface to accomplish this. The EW is an electromagnetic wave whose amplitude decreases dramatically as it travels through the internet. The metal surface is positioned nearer to the evanescent field by leaving an

air gap between the prism base and metal layer. However, since the metal must be placed within 200 nm of the prism surface, this design is difficult to implement in practice [43].

Kretschmann configuration

Kretschmann and Raether stated a prism based SPR configuration also in 1968 which is known as Kretschmann configuration for excitation. They noticed the metal layer's relation to the prism base. EW may be formed as a result of the prism-metal interaction in this case. The metal's thickness is once again reduced to an acceptable level. As a result, EW could also excite SPR at the metal dielectric interface. There are a number of ways to get around Otto's limits. One method is to coat a very thin metal layer of around 50 nm in direct contact with a dielectric medium with a lower refractive index. At the prism-metal interface, EW is formed. It is generated when the incident angle of polarized light equals or exceeds the critical angle. After that, it joins the metal and combines with SPW. Following that, it activates the SPR. The Otto configuration has certain disadvantages. The goal analytes are in contact with the metal surface, which is one of the remedies [44].

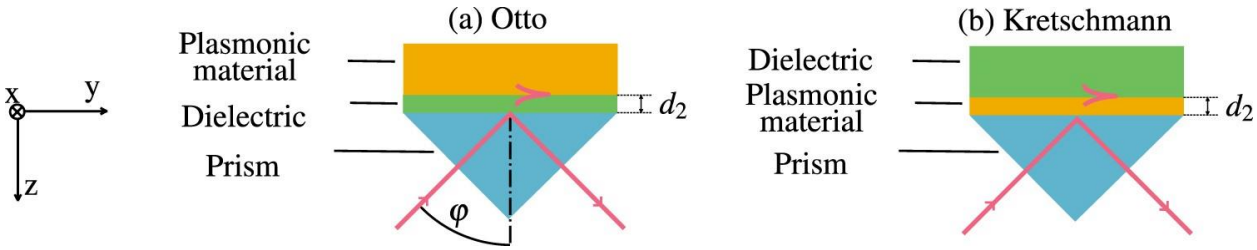

Figure 5.3: Excitation of SPR through Otto and Kretschmann configuration [45]

5.8 Types of SPR sensing

Two types of SPR sensing is used. Internal sensing and external sensing mechanism. Both were used in the past but at present external sensing mechanism is highly used.

5.8.1 Internal sensing mechanism

The metal coating and dielectric material are placed within the fiber in the internal sensing approach. This can be obtained, for example, by covering air holes with the dielectric liquid under investigation. One of the most important limitations of the interior detecting portion is the difficulty in topping off and exhausting selected air holes, which is extremely time consuming. This is the reason internal sensing mechanism isn't a good choice for practical purpose.

5.8.2 External sensing mechanism

Due to the limitations of the internal detecting device and detecting with a side washed PCF, the outer detecting system is appealing as a technique for practical applications. The dielectric material is placed in contact with the external metal surface of the PCF in an external detecting, which facilitates the cleaning and re-use of the fiber sensor with the corresponding dielectrics. As a result, external detection is used in useful situations where the benefits of the inner detecting device outweigh the disadvantages.

5.9 Factors beneath SPR sensing performance

SPR sensors provide a wide range of sensing efficiency depending on the specification parameters. As a result, in order to achieve the optimal performance, various parameters must be optimized to find the same value at which the greatest sensitivity occurs with the fewest losses. The results of such influential parameters on the sensing output are described in this section.

5.9.1 Plasmonic material thickness

The thickness of the plasmonic film affects the sensing efficiency significantly. It also has a major impact on the resonance wavelength change. Increasing it creates a change of the peak loss into a longer wavelength, as well as a reduction in the depth thickness of the loss. In addition, greater thickness leads to the evanescent field's lower entry. Furthermore, greater thickness leads to the evanescent field's lower entry to the atmosphere, resulting in reduced amplitude sensitivity. As a result, thickness and sensitivity have an inverse relationship. As the thickness of the layer is raised, the excited polaritons must migrate a greater distance to penetrate and communicate with the analyte. If the thickness of the material reduces, light penetration decreases, and the failure peak changes to a higher resonant wavelength [49].

5.9.2 Cladding and core air hole diameter

The amplitude sensitivity is affected by variations in cladding air gaps. It can be shown that changing the air hole diameter from its maximum causes the failure peak to widen and the amplitude sensitivity to decrease. The containment loss scales up as the diameter of the core air holes grows. And the n_{eff} gap between the core and the cladding shrinks as the depth of the core air hole becomes greater. As a consequence, there is a rise in loss [7].

5.9.3 Pitch distance

While there is no substantial difference in wavelength sensitivity as the pitch wavelengths are changed, there are significant differences in amplitude sensitivity. However, in some situations, as pitch size decreases, the resonant peak changes to a higher wavelength, and as pitch size increases, the resonant peak shifts to a lower wavelength. Since light is confined less closely with the central area as the pitch value increases, the loss peak changes towards the shorter wavelength with enhanced confinement loss value [49].

5.9.4 PML thickness

PML has a negligible effect on both containment failure and sensitivity. The decrement of PML thickness below 1.0 m resulted in a significant shift in amplitude sensitivity in our design, which will be presented in the following chapter, but PML thickness greater than 1.0m provided comparable sensing efficiency.

5.9.5 Analyte Refractive Index

The effect of RI on the sensing efficiency of the SPR sensor is the most important. The field penetration through the cladding region increases as containment loss increases. This indicates that the greatest amount of energy is transferred from the core driven mode to the SPP mode. The refractive index distinction between the core-guided mode and the SPP-mode reduces as the analyte RI rises, making the sensor more active. Since the length of a sensor is completely dependent on the absorption loss, increasing RI reduces the sensing length. As a result, as RI increases, the susceptibility peak changes to a higher resonance wavelength, broadening the overall curve.

5.10 Properties related to SPR

Fused Silica (SiO_2) is used for the reference and core materials in the optical fiber-based stimulation of SPR in general, as well as in the case of our thesis. Since the refractive index profile of silica is wavelength dependent, the Sellmeier equation is used. The dielectric constant of gold is calculated using the Drude-Lorenz formula.

5.10.1 Loss

In an SPR sensor, confinement loss is a critical guiding property. It is defined as the reduction caused by the standard cladding's finite magnitude. The number of layers, the number of air holes,

the depth of the air hole, and the pitch of the air hole will all affect confinement loss [46].The real part of the SPP mode's n_{eff} is heavily reliant on minor changes in the analyte's RI. A slight difference in the analyte RI causes a shift in n_{eff}, which is responsible for phase adjustment to other resonance wavelengths. When the RI is raised, the actual portion of the n_{eff} of the SPP mode shifts to a higher wavelength. When the core-guided prime mode and the SPP mode converge in phase matching state, a significant loss peak is observed at a particular wavelength. The full power is shifted from the core-guided prime mode to the SPP mode as a result of this directive. The deficit is also affected by minor changes in the RI index. For a slight rise in analyte's RI, the failure peak shifts dramatically to a higher wavelength.

5.10.2 Wavelength Sensitivity

The most important performance metric for SPR is sensitivity. The wavelength and amplitude inspection techniques can also be used to assess a sensor's sensitivity. The WS of a sensor can be measured using the wavelength interrogation procedure [47].As a result, the greater the distance between two successive resonant wavelengths, the greater the sensitivity.

5.10.3 Amplitude Sensitivity

Since it does not require wavelength interpolation, the amplitude interrogation method is less complicated and less expensive than the wavelength interrogation method. The amplitude of the failure peak varies as the analyte RI is modified. Since light is limited further as band gap increases, the amplitude sensitivity gradually rises while the core mode electric field penetrates the cladding area less [48]. Since the failure peak is sharper at x than y polarization, X-polarization normally has better amplitude response than Y-polarization.

5.10.4 Sensor Resolution

Sensor resolution determines the degree of detection with analyte RI variation. The resolution of a sensor can be determined by the resonance peak transfer, minimal wavelength resolution and

sensor resolution [51].The term "resolution" refers to a sensor's ability to detect a very small difference in RI on the order of 10^{-6}.

5.11 Advantages of SPR sensor

Though there are a variety of bio-detecting devices available, SPR technology makes monitoring restricted behavior on a sub-atomic level easier and more precise than any other mechanism. The followings are the major advantages of using SPR sensors:

Label Free Identification

SPR recognizes contrasts in the refractive background, so no name is needed for identification. We may observe the bio-subatomic cooperation between a variety of proteins, DNA or RNA, and small particles in real time.

Small in Sizes

To run experiments, SPR needs an insignificant level of examination. Researchers and medical professionals would be able to use less expensive components, saving money and making surface plasmon resonator more affordable and available.

Real Time Monitoring and Control

Essentially, using SPR technology allows researchers to see how different biomolecules interact over time in a simple and generally low-cost manner. This has a lot of uses in the medicinal and therapeutic industries, as well as in the fields of genetic qualities and electricity. New uses for materials, such as nanoparticles, are also a burgeoning field of research.

5.12 Applications of SPR sensors

SPR has earned popularity as a result of many promising applications. Bio-sensing, higher chemical identification accuracy, and environmental tracking are also affected significantly. Bio-imaging, liquid identification, medical disease verification, thin film thickness control all are

benefitted from SPR. Optoelectronic instruments like optical tunable filters, are now practically implementable due to research on SPR [50].Compound fume recognition is done using SPR. This occurs in the vaporous stage. SPR technology is now widely used for nourishment, environmental wellbeing, and other purpose.

Chapter 6

PCF based SPR sensor

6.1 Introduction

We explored more about photonic crystal fibers (PCF) and surface plasmon resonance throughout the early topics (SPR). A SPR sensor based on PCF is a photonic crystal fiber, which flaps the basic standard of the surface plasma resonance phenomenon. A SPR sensor based on PCF is a photonic crystal fiber, which flaps the basic standard of the surface plasma resonance phenomenon.

As an exceptionally sensitive adjustable development for the test compound and natural analytes, PCF-based SPR sensors were built up. PCF SPR distinguishing joins PCF growth and plasmonics in order to manage the short-term field and light expansion properties decisively, in individual or multimode action courses.

The PCFs consist of a core and a cover like standard optical fibers, but there are intermittent air outlines in the cladding region of PCFs that cope with the generating of light. Light diffusion through the PCFs follows the changed total internal reflection or impacts of photonic band holes. By changing air gaps and altering the quantity of loop, the light diffusion can be limited.

6.2 Preference of PCF based SPR sensors over Prism based

Depending on the point-cross test technology the crystal-based SPR sensors are controlled. The reverberation occurs at a specific point when the wave vector of EW and SPW is synchronized and a reflected wave is generated. In a certain point, it is difficult to send light every now and then. Moreover, it still has a huge structure. PCFs have shown exceptional consideration to address these problems since the last two decades. As a result of their minimal estimate and structural adaptability it is possible to efficiently monitor the transient area in PCFs. Streamlined calculation or positioning of the core reinforcing cladding, light is scattered in single mode, as is zero-rate light in the middle to energize surface plasmons. Single mode PCFs are highly sharp, which

upgrades the accuracy of detection. In addition, it is possible to extend its affectability and detection by updating the auxiliary parameters.

6.3 Sensing mechanism of PCF based SPR sensors

The regular functioning of PCF-based SPR sensors depends on the region. The electromagnetic field will somehow join in the cladding district by scattering light emission across the middle. The transient field in PCF SPR sensors penetrates the recessed region and is associated with plasmonic metal which activates free surface electrons. The surface plasmon wave is produced and generated along the metal dielectric surface at the point where reverberations occur. This state of reverberation leads to a close band disaster.

The most intense vitality transitions from central mode to SPP mode under a resonating environment. The modification to the dielectric medium (sample) refractive list results in a persuasive file shift in the SPP refractive mode, which causes the head of reverberation to decrease and the reverberating wavelength to travel. Dark convergence of an example may be recognized by the diversity of misfortune due to the variation in the refractive file of an analyte. Cross-examen techniques for wavelength and amplitude are known as important dissecting parameters for the execution of PCF-based SPR sensors.

6.4 Enhancing the sensitivity of PCF based SPR sensors

The responsiveness of the SPR sensors can be boosted by covering the PCF metal sheet to enhance fleeting field cooperation and free surface electrons.

Simple cooperation with the free metal layer electrons gives the center-guided connection to the SPP mode that enhances the execution of the sensor.

And that is how we can enhance the impact of SPR sensors depending on the PCF.

6.5 Advantages of PCF based SPR sensors

PCF-based SPR sensors have the key benefits following**:**

- They have feature robustness. PCFs have periodic air gaps in the cladding sector which address light development. By modifying the geometries of air openings and by adjusting the amount of the seal, the light spread can be restricted
- For analyte fixation estimates, PCF SPR sensors have high sensitivity and minimization.
- The center cover width and the field are optimized. It is diminished and can be merged in micro scale.

Chapter 7

Proposed Design, Simulation and Analysis

7.1 Introduction

The electromagnetic reaction that happens when polarized light reaches a metal film at the media interface with various refractive indices is referred to by Surface Plasmon Resonance and can be used to calculate the molecules' binding in real-time without using labels. Due to their easiness to implement and use, SPR-based technology with high sensitivity is very popular. They are also highly used because they do not require the use of labels to facilitate measurement and can benefit us with real-time identification of various bio-molecular interactions [52]. Localized Surface Plasmon Resonance (LSPR) sensors are seen as a new equivalent to well established SPR sensors among plasmonic sensors. LSPR based sensors are in growing demand, as they cost less and are convenient to use. Also their modification can be easily possible and they have a variety of applications.

Prism-based SPR sensors are used in popular scenarios. Prism causes the light to transfer to the surface interface of the metal, and the incident light is then absorbed by the independent electrons of the metal surface. As an outcome of this phenomenon a surface plasmon wave is produced. SPR sensor which is based on prism mechanism is large and takes up much space [52, 53].SPR sensor based on photonic crystal fiber is used to solve these problems. Due to their properties leading to lightweight, single-mode light guidance, geometry stability, high nonlinearity, unusual dispersion, tolerance to electromagnetic interference, and easily controlled elevated birefringence, PCF-based optical sensors are considered preferable [54-56].PCF also provides various applications in the sector of chemical detection. [57-61]

PCF SPR sensors operate based on the evanescent field produced by the spreading of light through the core-cladding interface. When core mode and surface plasmon polariton (SPP) mode are coupled with one another at a certain wavelength, PCF-based SPR sensors function. This specific wavelength is known as resonance wavelength, where the effective RI real part is identical for both core mode and SPP mode. Since the SPP mode is susceptible to the neighboring insulating layer's

RI, the phase-matching condition relies heavily on the analyte RI [62]. If the analyte refractive index (RI) increases, then there will be a change in the real part of the effective surface plasmon polariton index of the nearby surface. Because of this, there will also be a change in resonant wavelength. Through measuring this shifting of resonant wavelength, the particles or molecules can be detected correctly. This is the underlying principle of the PCF SPR sensors [63, 64]. LSPR is the result of surface plasmon excitation that occurs in small metals or nanoparticles, which may significantly strengthen the sensing mechanism. LSPR can directly detect refractive index of its target and can be used for multiplex sensing.

PCF sensor can be based on either an internal sensing mechanism or external sensing mechanism. In the case of an internal sensing mechanism, air holes are filled with an analyte, and in the case of an external sensing mechanism analyte is positioned at the surface of a PCF. We have seen some recent works based on internal sensing mechanism [65]. However, it has some drawbacks. The internal sensing mechanism is problematic for the filling and the flushing of the analyte as it takes a lot of time [66]. It is also not suitable for applications with real-time and remote sensing. For internally metal-coated PCF-SPR sensors, Fabrication is difficult as it requires analyte coating on the surface of the narrow air hole [67]. An improved method was established by using the D-shaped structure [68-70]. Although it is easy to clean a D-shaped structure for analyte refilling, it is also challenging in practical aspects [2]. That is why, in recent times, the external sensing approach is highly used. Any of these can be used as plasmonic materials among gold, silver, copper. Silver provides a sharper resonance peak, but silver and copper can be readily oxidized in humid environments, decreasing analyte detection accuracy [71, 3]. As gold is chemically stable and, therefore, provides substantial resonance peaks [72]. Numerous works have also been conducted using gold as plasmonic material.

In view of the above discussions, we implemented a gold-coated PCF-LSPR sensor using an external sensing mechanism. Our proposed configuration included two V-shaped stacks of air holes identical in height. This design has a strong sensitivity with a low loss that can increase the absorption, resolution, and detection limit.

7.2 Structural design of our proposed sensor

The layout and the numerical analysis of the sensor are done by using COMSOL Multiphysics 5.3. Mesh sequence regulated by physics to attain optimum accuracy in simulation, here extremely fine simulation is used. Figure 7.1 indicates the cross-sectional view of our proposed sensor. In the cladding part, we are using two V-shaped clusters. They are located exact reverse to each other across the horizontal plane. Each has nine circular air holes that help us pass the light center to create a strong photoluminescence impact on the metal. It consists of two different diameters of air hole rings. The air hole of each V-shaped cluster is larger than the center air hole. Here d_c=0.396um is the diameter of center air hole and d_1=1.3um is the diameter of the rest air holes, and t_g = 30nm is the thickness of the gold layer. The distance between two adjoining air holes is defined by Λ. The numerical value of our proposed sensor pitch size Λ=1.345μm. In our proposed design, we use gold as a plasmonic metal where gold shows more chemical stability than other metals. We use a skinny gold layer which adept an island growth. Here, the backdrop substance is fused silica.

The substance scattering of pure silica can be calculated by using the sellmeier equation. [73]:

$$n_{silica} = \sqrt{1 + \frac{0.69616\lambda^2}{\lambda^2 - 0.00467914} + \frac{0.40794\lambda^2}{\lambda^2 - 0.013512063} + \frac{0.89747\lambda^2}{\lambda^2 - 97.93400253}} \tag{7.1}$$

Where, n_{silica} denotes to the RI of silica and λ denotes to the wavelength of light.

In the top layer of photonic crystal fiber, a thin gold layer t_g= 30nm is deposited. The gold coating has a massive impact on the sensing capabilities of a sensor located on the surface of the Photonic Crystal Fiber module. It is possible to realize the dielectric function of gold by Drude-Lorentz model [67]:

$$\varepsilon_{AU} = \varepsilon_{\infty} - \frac{{\omega_0}^2}{\omega(\omega + j\gamma D)} - \frac{\Delta\varepsilon.{\Omega_L}^2}{\left(\omega^2 - {\Omega_L}^2\right) + j\Gamma_L\omega} \tag{7.2}$$

Where, $\varepsilon_{\infty} = 5.9673$ indicates the permittivity of high frequency, $_{\triangle}\varepsilon = 1.09$ indicates the weighting vector. ω is the angular frequency, where numerical values of $\omega_D = 4227.2\pi$ THz represents the

plasma frequency and $\gamma_D =$ 31.84π THz represents damping frequency. Accordingly, the spectral width $\Gamma_L =$ 209.72π THz and oscillator strength is $\Omega_L =$ 1300.14π THz.

The RI of TiO_2 is calculated by using this equation [74]:

$$n_t = \sqrt{5.913 + \frac{2.441\times10^7}{\lambda^2 - 0.803\times10^7}} \tag{7.3}$$

Where n_t indicates the RI of TiO_2.

In our proposed sensor, we use a finite element solution with a strong radiation absorber. It's precisely matched with the boundary state on the outermost layer. The dispersing boundary condition of the outermost layer is used to scrutinize the confinement mode.

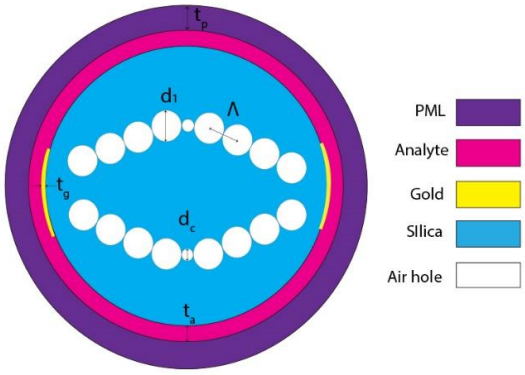

Figure 7.1: 2D schematic cross sectional view

7.3 Optimization, result, and performance analysis

For our proposed sensor, we first optimize the different structure and operating parameters of the design in a specific RI, which was 1.37. After that, we analyze the sensor activity by changing the analyte RI to find the best possible outcome from this design. The optimization method entails holding all parameters constant and changing a parameters one after one [75]. Initially, both X and Y polarization are analyzed, but Y polarization is chosen for further investigation because Y polarization has better results than X polarization. We calculated CL, WS, AS, Resolution, and

FOM in different RI to determine the optimized performance result and the next possible approach throughout our optimization process.

The following equation gives the CL relationship [76]:

$$\alpha_{loss} = 8.686 \times \frac{2\pi}{\lambda} \times I_m\left(reff\right) \times 10^{2\ dB/m} \tag{7.4}$$

Here, $I_m\left(reff\right)$ is the imaginary part of the complex refractive index of the core guided mode.

The following equation can derive sensitivity by wavelength interrogation method [20]:

$$S_\lambda \left(nm/RIU \right) = \Delta\lambda_{peak} / \Delta n_a \ \ dB/cm \tag{7.5}$$

Here, $\Delta\lambda_{peak}$ denotes the peak wavelength shifting and Δn_a is the change in dielectric RI.

Amplitude sensitivity (AS) is another crucial parameter to assess sensor output, and the following equation determines it [77]:

$$S_A = -\frac{1}{\alpha\left(\lambda, n_a\right)} \frac{\partial\alpha\left(\lambda, n_a\right)}{\partial n_a} \left(RIU^{-1}\right) \tag{7.6}$$

Here, $\partial\alpha\left(\lambda, n_a\right)$ indicates the difference between two-loss spectra due to small change of analyte RI when $\alpha\left(\lambda, n_a\right)$ is the overall propagation loss at a specific RI.

The degree of detection with RI variation is measured by sensor resolution that depends on the sensor sensitivity. The following equation determines it [78]:

$$R_\lambda = \frac{\partial n_a \times \partial\lambda_{\min}}{\partial\lambda_{peak}} \left(RIU\right) \tag{7.7}$$

Where ∂n_a represents a variation in analyte RI, $\partial\lambda_{\min}$ defines the minimum wavelength resolution, and $\partial\lambda_{peak}$ decides the resonance peak shift difference.

In addition to amplitude sensitivity, wavelength sensitivity and resolution, the output of the sensor can also be indicated by another parameter known as the figure of merit (FOM), which is simply the WS and FWHM ratio. The FOM can be determined by following equation if S_λ is the WS and FWHM is full width at half-maximum [79]:

$$FOM = \frac{S_\lambda \left({}^{nm}/_{RIU} \right)}{FWHM \left(nm \right)} \tag{7.8}$$

Amplitude sensitivity is the major issue for this sensor since it does not require spectrum tracking. Therefore, it is cost-effective and easy to measure. [80].

7.3.1 Pitch, air cavity, and air hole diameter

Our sensor core consists of only circular air holes as it is easy to fabricate [81]. The air hole diameters are chosen in such a way so that the light is entirely squeezed in the central area. We chose d_1=1.3µm. Increasing the value of d_1 would result in overlapping of air holes and creating fabrication problems. Besides, the confinement area within the core decreases so that a sufficient evanescent field cannot be produced to electrify the metal layer's surface plasmons [82]. Reducing this value increases CL because of the leaky mode of PCF [76].

Another air hole diameter d_c=0.396µm. AS gets maximum for this d_c value. It is the proper size to generate a robust mutual connection between core guided mode and SPP mode.

After choosing the air hole sizes, we get the pitch value Λ=1.345µm, which helps the core mode interact correctly with the plasmonic metal. Substantial plasmonic quality is a sign of reaching high wavelength sensitivity [83]. Arranging the air holes in a specific position gives the perfect air cavity for tapping the light inside the core. Selecting these diameters and keeping these air holes in their respective positions helps attain high performance from this sensor. The electric field distribution and the guiding property of our design can be observed in figure 7.2.

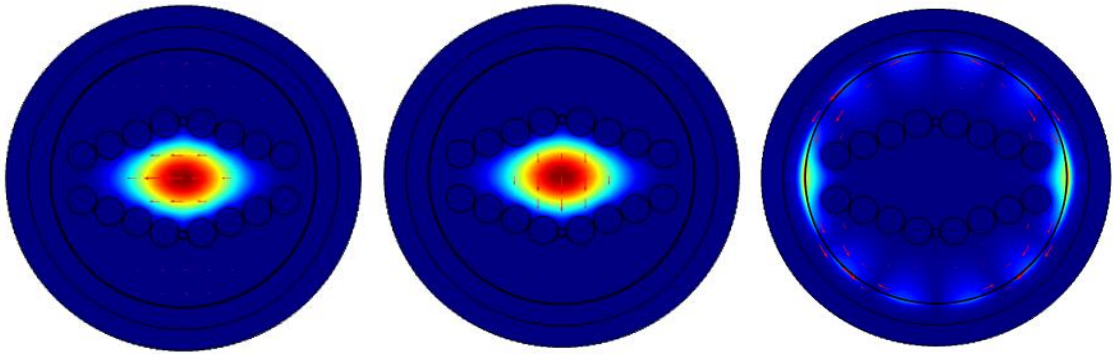

(a) (b) (c)

Figure 7.2: EM field confinement of fundamental core mode (a) X-polarization, (b) Y-polarization, and (c) SPP-mode

7.3.2 Dispersion relation

In figure 7.3, the dispersion relation of RI=1.37 is shown. As the incident light wavelength raises, the real part of refractive index (n_{eff}) of both core and SPP modes reduce. The CL reaches its maximum at the same RI point of the core and SPP modes, which is 0.61μm in our case, and this CL peak is appropriate for easy and efficient analyte sensing [83]. This phase matching point is termed as resonance wavelength, which satisfies the theoretical condition for SPR. Significant energy distribution from core mode to SPP mode occurs at this point [82].

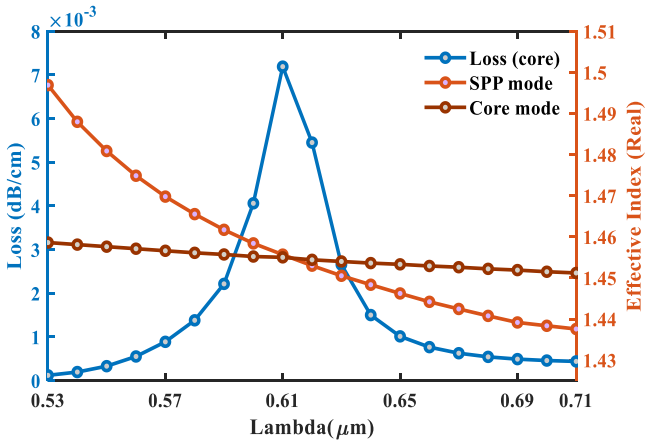

Figure 7.3: Dispersion Relation

7.3.3 Impact of Gold & TiO_2 layer thickness variation

First, we optimize the gold layer thickness, which strongly impacts the loss, RW change, and sensing ability of a PCF sensing process [83]. We started our optimization by keeping t_g= 30 nm and then checked the impact of changing this parameter. As t_g increases, the loss peak is widening, increasing the FWHM while decreasing the FOM. A fine t_g layer enables easy interaction between the analyte and evanescent field which increases sensitivity [75]. However, a fragile gold layer also reduces the sensitivity because of surface plasmons' skin depth restriction [52, 63]. Different t_g layer output is shown in figure 7.4 in terms of loss & amplitude sensitivity. While t_g= 29 nm gives the AS value of 474 RIU^{-1} keeping the CL value equal to 0.0066 dB/cm & 0.0096 dB/cm for RI= 1.37 & 1.38 respectively, t_g = 31 nm gives 504 RIU^{-1} AS value and 0.0073 dB/cm & 0.0086 dB/cm CL values. Nevertheless, the highest AS found 510 RIU^{-1} for t_g =30 nm when the CL values are 0.0072 dB/cm and 0.0092 dB/cm. Considering the moderate CL and highest AS, we chose 30 nm as our optimum value.

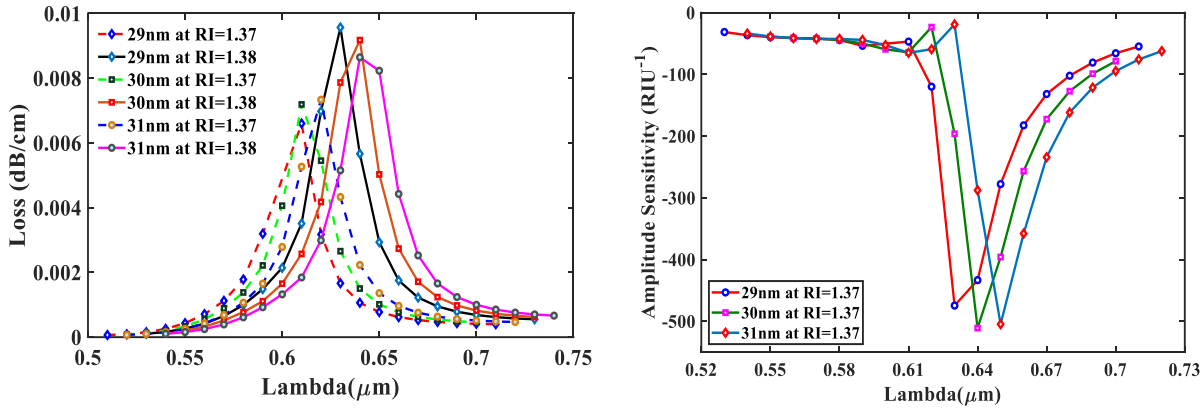

(a) (b)

Figure 7.4: (a) CL curves varying gold layer thickness (t_g) at analyte RI=1.37 & 1.38; (b) AS curves varying gold layer thickness (t_g) at analyte RI=1.37

Keeping t_g= 30 nm, we changed the TiO_2 layer thickness and checked the impact. Generally, the TiO_2 layer is used to lessen Au's adhesion problem [83], but in our case, the TiO_2 layer significantly reduces the AS value, which is our main priority for this sensor. Figure 7.5 shows that without the TiO_2 layer, we get the AS value of 510 RIU^{-1}, and with the TiO_2 layer, it goes down to 466 RIU^{-1} when CL values for both the cases are almost similar. Only 0.0001 dB/cm difference for both RI=

1.37 & RI= 1.38. So, we moved forward in our designing procedure, keeping TiO2 layer thickness= 0 nm.

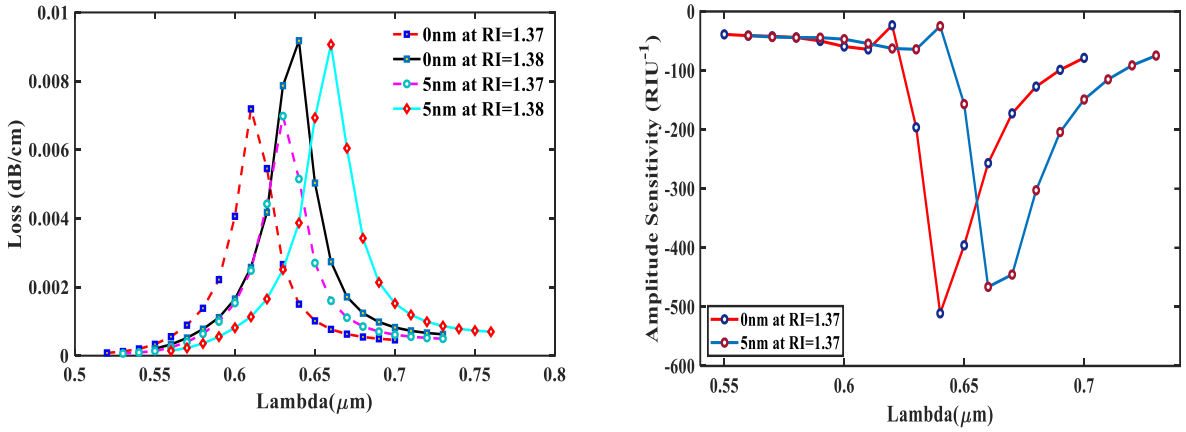

(a) (b)

Figure 7.5: (a) CL curves varying TiO_2 layer thickness (t_t) at analyte RI=1.37 & 1.38; (b) AS curves varying TiO_2 layer thickness (t_t) at analyte RI=1.37

7.3.4 Metal grating performance analysis

Metal grating is the localization of SPR, which is called LSPR. Our next optimization was based on these SPR and LSPR performance. From figure 7.6, we can see that we get the AS value of 510 RIU^{-1} when it is a metal layer (SPR) and 597 RIU^{-1} when it is metal grating (LSPR) though the loss increased from 0.0072 dB/cm to 0.0083 dB/cm and 0.0092 dB/cm to 0.01 dB/cm. As the main parameter AS is higher, we proceed further in our optimization process with metal grating.

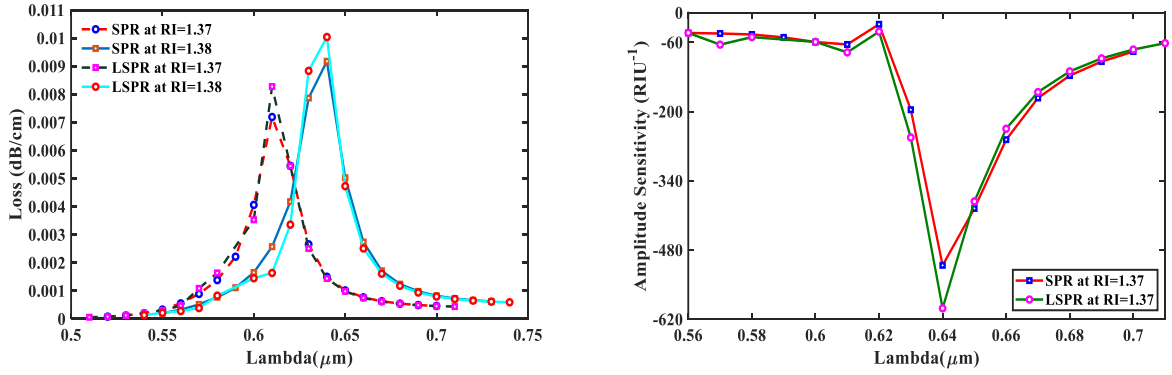

(a) (b)

Figure 7.6: (a) CL curves for SPR and LSPR at analyte RI=1.37 & 1.38; (b) AS curves for SPR and LSPR at analyte RI=1.37

7.3.5 Impact of varying the thickness of different layers

We tried to see the variation of sensing performance with analyte layer thickness change. Figure 7.7 shows the impact of varying analyte thickness t_a. When t_a=0.6um, we get the AS value of 617 RIU^{-1}. As the thickness increases, a stable relationship between the evanescent field and the analyte is established, increasing AS. So, when t_a=0.65 um, the AS becomes 630 RIU^{-1} though loss values are almost similar. The thickness further increases to 0.7um, but the AS reduces to 625 RIU^{-1} keeping the CL values almost constant. The fundamental explanation for this reduction in AS is that a thick t_a layer expands the light in a vast region; thus, the coupling competence decreases, and AS reduces [84]. It also weakens the relationship between the evanescent field and analyte [83]. Considering the AS value, 0.65 um is chosen as the optimum value for the analyte layer.

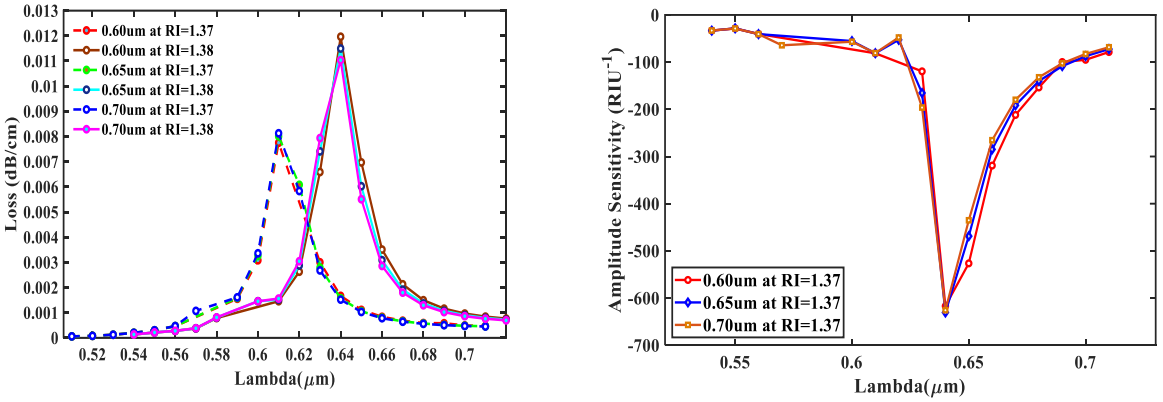

(a) (b)

Figure 7.7: (a) CL curves varying analyte layer thickness (t_a) at analyte RI=1.37 & 1.38; (b) AS curves varying analyte layer thickness (t_a) at analyte RI=1.37

Finally, PML layer thickness also extended to 1, 1.05, and 1.1 um to find the sensing performance variation. The characteristics curve is shown in figure 7.8. We can see that the PML layer has minimal impact on the confinement loss parameter. For t_p=1um, the AS we found was 630 RIU^{-1}. With the increase of t_p, the AS increases to 631 RIU^{-1} when t_p=1.05um. The t_p value of more than 1.05um provides the close result as shown for t_p=1.1um when the AS value we found was 630 RIU^{-1}. Taking the AS value and sensor size into account, 1.05 um is selected as PML layer thickness.

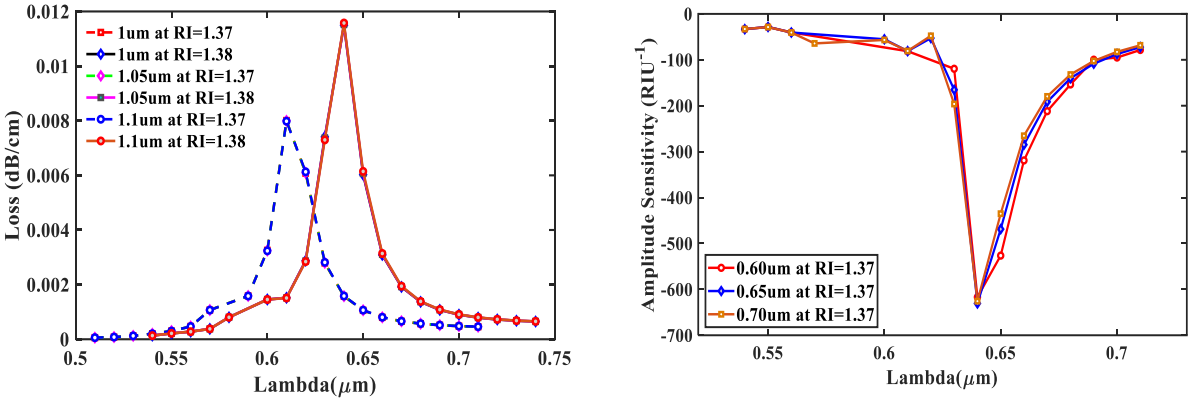

(a) (b)

Figure 7.8: (a) CL curves varying PML layer thickness (t_p) at analyte RI=1.37 & 1.38; (b) AS curves varying PML layer thickness (t_p) at analyte RI=1.37

7.3.6 Sensor performance evaluation

The wavelength range we consider for our simulation was 0.45um to 0.95um with an interval of 0.01. The sensor performance was evaluated in the RI range of 1.33-1.41 due to its potential use in biological sample testing. A variety of biochemical compounds have a RI in the defined range that our sensor can sense. For example, silicone oil-1.403, acetone-1.36, liver (human)-1.369, glucose solution in water-1.347 to 1.364, intestinal mucosa (human)-1.338 etc. [85]. The maximum shift in RW is obtained in this RI range. Here, all the sensor's performance evaluation was based on the change of RI of the core guided mode.

Fig. 7.9(a) exhibits the CL spectrum of the proposed sensor. It is shown that CL increases with an increase in analyte RI, and the resonance peak goes to a higher value because of the propagation constant and kinetic energy change [84]. The lowest loss we found was 0.03 dB/cm at RI=1.33, and the highest CL we found was 0.11 dB/cm at RI=1.41.

The alteration of the analyte RI not only changes the CL, it also alters the AS property of the sensor. Figure 7.9(b) offers detailed data about amplitude sensitivity variation with the change of analyte refractive index. It is irrefutable that the AS is related to RI, and increasing RI results in improving AS. In the RI range of 1.33 to 1.38, AS increases slightly, but for 1.39 to 1.4, it displays a sharp rise. Lowest AS is found 220.83 RIU^{-1} at RI=1.33 and the highest 4779.7 RIU^{-1} at RI=1.40.

In addition to AS, the sensor performance also followed through the wavelength sensitivity measurement mentioned in equation 5. In contrast to most other developed SPR based sensors, this one displayed a high average wavelength sensitivity. An extremely sharp WS of 14000 nm/RIU was found between RI 1.40 to 1.41 because of the massive resonance wavelength change. This high sensing value is a sign of a better sensing precision, implying magnificent resolution, which indicates an excellent sensor [83]. The highest resolution we found is 7.14×10^{-6}. That means a small disturbance of the order 10^{-6} can be detected preciously by the proposed sensor.

Besides AS, WS, and resolution, this LSPR sensor shows an impressive FOM result, which characterizes the overall performance. A high-performance sensor can be recognized when AS & WS increase and FWHM decreases [85]. The Proposed sensor shows exceptional FOM values, such as the value 420 at analyte RI of 1.4. Be noted that a greater FOM indicates a better sensing quality.

All the parameters mentioned above (AS, WS, resolution, FOM, and FWHM) in all RI are shown in the table 7.1, and a detailed performance review of the proposed sensor with the previously proposed sensors is shown in the table 7.2.

Given the simplicity of the design, low CL values, and overall effectiveness, it is obvious that the proposed sensor has enhanced performance over the previously mentioned other sensors, which also fulfills our design objective of creating a practical LSPR biochemical sensor.

Table 7.1: Result analysis of the sensor based on AS, WS, Resolution and FOM

RI	AS (RIU^{-1})	WS (nm/RIU)	Resolution (AS)	Resolution (WS)	FWHM	FOM
1.33	220.8337	1000	4.53E-05	0.0001	23.16676	43.16
1.34	275.5551	2000	3.63E-05	0.00005	25.60416	78.11
1.35	334.6812	1000	2.99E-05	0.0001	24.78069	40.35
1.36	431.9583	2000	2.32E-05	0.00005	24.59524	81.32
1.37	631.0292	3000	1.58E-05	3.33E-05	24.78475	121.04
1.38	863.5396	3000	1.16E-05	3.33E-05	24.60256	121.94
1.39	1622	6000	6.17E-06	1.67E-05	27.11251	221.3
1.40	4779.7	14000	2.09E-06	7.14E-06	33.30416	420.37

Table 7.2: Comparison in terms of sensitivity, resolution and refractive index range of the proposed sensor with the prior sensors**.**

Ref.	RI Range	Max.AS (RIU^{-1})	Max.WS (nm/RIU)	Resolution (RIU)
[6]	1.33-1.38	420.4	4600	2.17×10^{-5}
[86]	1.40-1.44	739.26	9600	1.04×10^{-5}
[15]	1.46-1.475	820	23000	4.35×10^{-6}
[20]	1.33-1.37	860	5000	4×10^{-5}
[87]	1.33-1.40	1085	9000	1.11×10^{-5}
[83]	1.33-1.40	1189.5	13000	7.69×10^{-6}
[70]	1.36-1.41	1222	14660	6.82×10^{-6}
[88]	1.33-1.42	1420	11000	9.1×10^{-6}
Proposed	1.33-1.40	4779.7	14000	7.14×10^{-6}

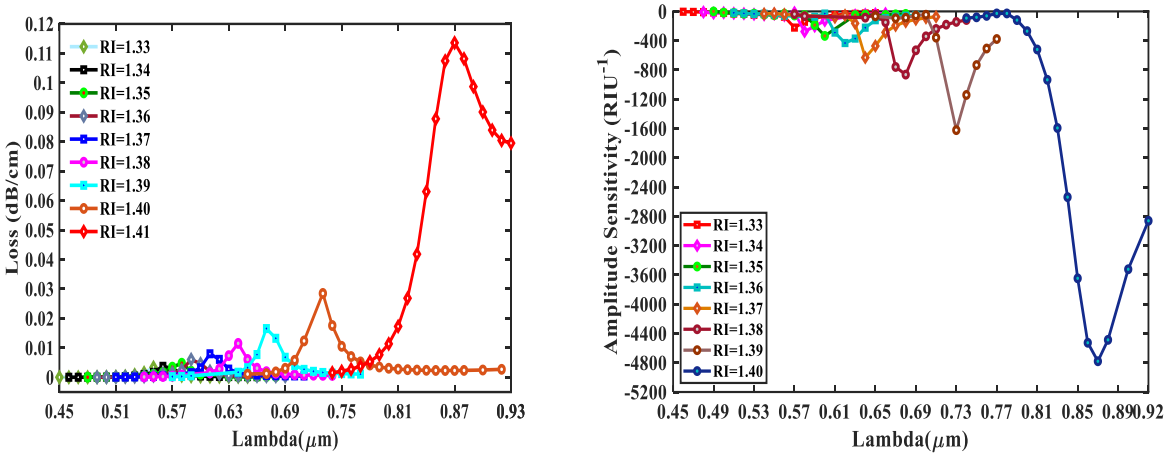

(a) (b)

Figure 7.9: (a) CL curves varying analyte RI with all optimized parameters; (b) AS curves varying analyte RI with all optimized parameters

7.3.7 Sensor length and linearity check

The length of the sensor depends on its CL values, which follows the following formula [79]:

$$L = 1/\alpha(\lambda,na) \tag{7.9}$$

$\alpha(\lambda,na)$ = peak confinement loss at a particular wavelength/alternation constant

Figure 7.10(a) shows that as RI increases, CL increases, resulting from the reduction in sensor length. According to the analysis, it can be claimed that a sensing range of small mm values to cm values can be utilized in practical sensing applications.

In linearly checking, we tried to develop a relationship between RW and RI. Fig. 7.10(b) manifests the relationship between the linear response of our sensor and analyte RI. The regression equation Y= -2.3167+2.1429X and R^2=0.97 assimilates a magnificent result.

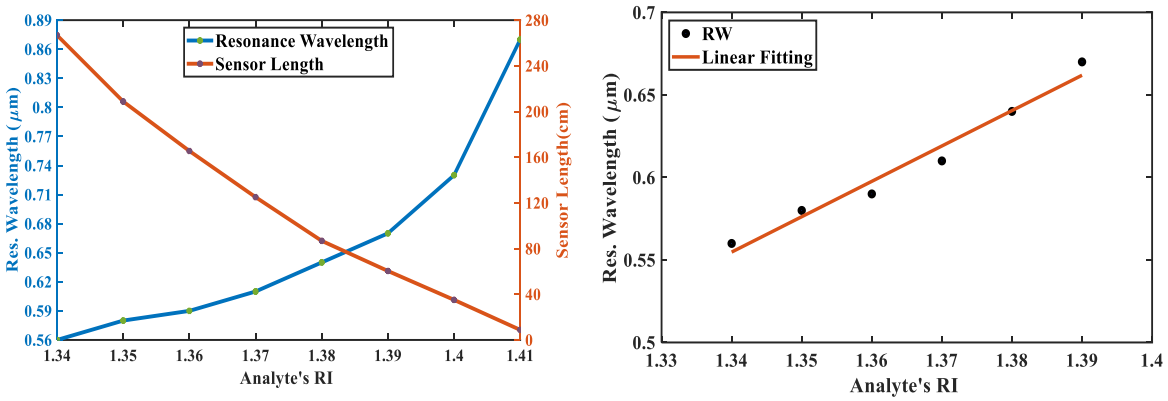

(a) (b)

Figure 7.10: (a) Resonance wavelength and sensor length varying analyte RI with all optimized parameters; (b) linearity response of the proposed sensor

7.4 Discussion

This research computationally elucidates the photonic crystal fiber biosensor. The complete vector finite element practice is used to investigate guidance characteristics. A perfectly aligned ring - shaped coating has been used to expel the exposure to the surface. The proposed sensor shows the maximum wavelength amplitude sensitivity of 14000nm/RIU using wavelength interrogation and 4779.7 RIU -1 using the amplitude interrogation method. The resistance of the make, which ranges by 10 percent, shows no significant reaction curve shifts. The proposed system has a multitude of applications for biochemistry- and biological analyte detection in laboratory fiber technology due to the manufacturing viability and the extremely sensitive results.

Chapter 8

Conclusion, Impact and Future Work

8.1 Conclusion

In this research, we tried to develop a PCF-based SPR sensor. These sensors are essential to sense biochemical and bimolecular agents. They are small in size, and the light propagation mechanism can be controlled, eliminating the drawbacks created by the previous prism-based SPR sensor. Different plasmonic materials are used for sensing purposes based on the activity. Guiding properties are numerically investigated by commercial COMSOL software. The value of sensitivity defines how precisely a sensor can sense, and it is determined by wavelength interrogation method and amplitude interrogation method.

In our thesis, we proposed a hollow core LSPR sensor which is simple in design and effective in sensing. This sensor offers high sensitivity and improved resolution. Here, gold is used as plasmonic material. Both analyte layer and gold film are positioned at exterior surface of the PCF. The prime reasons are to minimize the fabrication difficulty and to have more practical sensing. Proposed sensor shows maximum wavelength sensitivity 14000 nm/RIU and amplitude sensitivity 4779.7 RIU^{-1}. Resolution of this PCF based SPR sensor is 7.14×10^{-6} RIU. It also shows admirable linear properties. To our knowledge, this is the highest sensitivity for an LSPR sensor in published literature, and facilitates future development for accurate and precise analyte measurement and the high resolution indicates its usages in biological and biochemical analytes detection. It has practical simplicity, suitable linearity and excellent sensing qualities.

8.2 Socio-Economic Impact

This research work has a great impact on our economy as well as our society and can be considered as a successful one as it offers a sensor with high sensitivity and low loss. This sensor can be used in medical research such as detecting plasma, blood from an unknown sample. In chemical research it helps to determine the presence of harmful gases in a complex mixture. Besides, this

simple and effective work motivates others to continue research in designing more sensitive PCF based SPR sensors.

8.3 Future Work

PCF SPR is a promising and competitive sensing technology. However, at the device development front, PCF SPR sensors are still in early age. There are some works needed to do for the better improvement. In future in order to investigate further we will do the following:

•Since we are interested in the field of sensing applications, our primary focus for future work would be to enhance the sensitivity of our proposed model.

•Due to fabrication challenges, PCF based sensors have limited practical applications. Most of the investigations are performed theoretically. Simulation model is also greatly used. So, experimental research for using PCF sensors in real-world appliances can be a dynamic upcoming research.

•For detecting large amount of biological and biochemical analytes, PCF based sensor which can sense numerous refractive indices can be examined in future.

•As PCF-based sensors are mainly employed in lab-oriented researches, in future commercialization of the sensors can be improved.

•For future progress it is possible to implement this design by adding alternative plasmonic material outside the PCF surface.

•Same design can be implemented on D-shaped PCF and also using different shape air holes. Internal and external sensing approach with the same design can be examined.

•SPR sensing technologies for THz frequencies can be improved. Moreover, in future, new design with improved performance can be implemented.

•We are also very much interested to work with temperature sensors since fiber based temperature sensors are not affected by electromagnetic interference and RF.

References

[1] M. R. Momota and M. R. Hasan, "Hollow-core silver coated photonic crystal fiber plasmonic sensor," Optical Materials, vol. 76, pp. 287-294, Feb.2018.

[2] J. N. Dash and R. Jha, “On the performance of graphene-based D-shaped photonic crystal fibre biosensor using surface plasmon resonance,” Plasmonics, vol. 10, no. 5, pp. 1123-1131, 2015.

[3] A. A. Rifat, R. Ahmed, A. K. Yetisen, H. Butt, A. Sabouri, G. A. Mahdiraji, S. H. Yun and F. M. Adikan, “Photonic crystal fiber based plasmonic sensors,” Sensors and Actuators B: Chemical, vol. 243, pp. 311-325, May 2017.

[4] J. Homola and M. Piliarik, “Surface Plasmon Resonance (SPR) Sensors,” In Surface plasmon resonance based sensors, pp. 45-67, 2006.

[5] R. K. Gangwar and V. K. Singh, “Highly sensitive surface plasmon resonance based D-shaped photonic crystal fiber refractive index sensor,” Plasmonics, vol. 12, no. 5, pp. 1367-1372, 2017.

[6] M. R. Hasan, S. Akter, A. A. Rifat, S. Rana, K. Ahmed , R. Ahmed, H. Subbaraman and D. Abbott, “Spiral Photonic Crystal Fiber-Based Dual-Polarized Surface Plasmon Resonance Biosensor,” IEEE Sensors Journal, Vol. 18, no. 1, pp. 133-140, Jan. 2018.

[7] A. A. Rifat, G. A. Mahdiraji, Y. M. Sua, Y. G. Shee, R. Ahmed, D. M. Chow and F. M. Adikan, “Surface plasmon resonance photonic crystal fiber biosensor: a practical sensing approach,” IEEE Photonics Technology Letters, vol. 27, no. 15, pp. 1628-1631, Aug. 2015.

[8] M. R. Hasan, S. Akter, K. Ahmed and D. Abbott, “Plasmonic refractive index

sensor employing niobium nanofilm on photonic crystal fiber," IEEE Photonics Technology Letters, vol. 30, no. 4, pp. 315-318, Feb. 2018.

[9] A. A. Rifat, M. R. Hasan, R. Ahmed and H. Butt, "Photonic crystal fiber-based plasmonic biosensor with external sensing approach," Journal of Nanophotonics, vol. 12, no. 1, pp. 012503, Jun. 2017.

[10] E.K. Akowuah, T. Gorman, H. Ademgil, S. Haxha, G.K. Robinson, J.V. Oliver, Numerical analysis of a photonic crystal fiber for biosensing applications, IEEE J.51 Quantum Electron. 48 (2012) 1403–1410.

[11] Y. Lu, et al., SPR sensor based on polymer photonic crystal fibers with metal nanolayers,Sensors 13 (Jan. 2013) 956–965

[12] E.K. Akowuah, et al., A highly sensitive photonic crystal fibre (PCF)surface plasmon resonance (SPR) sensor based on a bimetallic structureof gold and silver, Proc. IEEE 4th Int. Conf. on Adaptive Scienceand Technology, 2012, pp. 121–125

[13] Z. Tan, et al., Improving the sensitivity of fiber surface plasmon resonance sensor by filling liquid in a hollow core photonic crystal fiber, Plasmonics 9 (1) (2014)

[14] Md. Selim Habib, Md. Samiul Habib, and S.M.A. Razzak, "Study on dual-concentriccore dispersion compensating photonic crystal fiber," International J. of Eng. and Technol., vol. 1, no. 4, pp. 377-383, 2012

[15] A. A. Rifat, G. A. Mahdiraji, Y. M. Sua, R. Ahmed, Y. G. Shee and F. M. Adikan, "Highly sensitive multi-core flat fiber surface plasmon resonance refractive index sensor," Optics express, vol 24, no. 3, pp. 2485-2495, Feb. 2016.

[16] K. Sharma, R. Jha and B. D. Gupta, "Fiber-optic sensors based on surface plasmon resonance: a comprehensive review," IEEE Sensors Journal, vol. 7, no. 8, pp. 1118-1129, Aug. 2007

[17] K.M. McPeak, S.V. Jayanti, S.J. Kress, S. Meyer, S. Iotti, A. Rossinelli et al, “Plasmonic films can easily be better: rules and recipes,” ACS Photonics, vol. 2, pp. 326–333, 2015.

[18] D. Gao, C. Guan, Y. Wen, X. Zhong and L. Yuan, “Multi-hole fiber based surface plasmon resonance sensor operated at near-infrared wavelengths,” Optics Communications, vol. 313, pp. 94-98, 2014.

[19] P. Bing, J. Yao, Y. Lu, Z. Li, “A surface-plasmon-resonance sensor based on photoniccrystal-fiber with large size microfluidic channels," Opt. Appl, vol. 42, pp. 493–501, 2012

[20] J.N. Dash and R. Jha, “Graphene-based birefringent photonic crystal fiber sensor using surface plasmon resonance,” IEEE Photonics Technology Letters, vol. 26, no. 11, pp. 1092-1095, June 2014

[21] R. Buczynski, “Photonic Crystal Fibers,” International School of Semiconducting Compounds, vol. 106, no. 2, pp. 141-168, Jun. 2004.

[22] Philip Russell, “Photonic Crystal Fibers: A Historical Account,” IEEE Leos Newsletter, vol. 21, no. 5, pp. 11-15, Oct. 2007.

[23] D. Ferrarini, L. Vincetti, M. Zoboli, A. Cucinotta, and S. Selleri, “Leakage properties of photonic crystal fibers,” Optics Express, vol. 10, no. 23, pp.1314-1319, 2002.

[24] G. P. Agrawal, “Nonlinear Fiber Optics,” Academic Press, 2nd Edition, 1995.

[25] S. Chowdhury, S. Sen, K. Ahmed, B.K. Paul, M.B.A. Miah, S. Asaduzzaman, M.S. Islam, M.I. Islam, Porous shaped photonic crystal fiber with strong confinement field in sensing applications: design and analysis, Sens. Bio-Sens. Res. 13 (1) (2017) 63–69.

[26] Md. Selim Habib, Md. Samiul Habib, S.M. Abdur Razzak, Yoshinori Namihira, M.A. Hossain, and M.A. Goffar Khan, “Broadband dispersion compensation of conventional single mode fibers using microstructure optical fibers,” Optik, vol. 124, no. 19, pp. 3851- 3855, Oct. 2013.

[27] M. A. Habib and M. S. Anower, "A Novel Low Loss Porous-Core Photonic Crystal Fiber for Terahertz Wave Transmission," in International Conference on Electrical, Computer and Communication Engineering (ECCE), Cox’s Bazar, Bangladesh, 2017.

[28] L. Chaudhary, A. Jb, and H. Purohit, “Photonic Crystal Fibre : Developments , Properties and Applications in Optical Fiber Communication,” International Journal for Research in Applied Science & Engineering Technology (IJRASET), vol. 5, no. Xi, pp. 1828–1832, 2017.

[29] R. Islam, G. K. M. Hasanuzzaman, M. S. Habib, S. Rana, and M. A. G. Khan, “Low-loss rotated porous core hexagonal single-mode fiber in THz regime,” Opt. Fiber Technol., vol. 24, pp. 38–43, 2015.

[30] I. K. Yakasai, A. Rahman, P. E. Abas, and F. Begum, “Theoretical Assessment of a Porous Core Photonic Crystal Fiber for Terahertz Wave Propagation,” Opt. Commun., pp. 1–11, 2018.

[31] J. Sultana et al., “Highly birefringent elliptical core photonic crystal fiber for terahertz application,” Opt. Commun., vol. 407, pp. 92–96, 2017.

[32] S. Ali et al., “Guiding properties of a hybrid core porous fiber (HCPF) for terahertz wave propagation,” 2nd International Conference on Electrical, Computer & Telecommunication Engineering (ICECTE), 2016, Rajshahi-6204, Bangladesh.

[33] M. R. Hasan, S. Ali, and S. A. Emi, “Ultra-low material loss microstructure fiber for terahertz guidance,” Photonics Lett. Pol., vol. 9, no. 2, pp. 66–68, 2017.

[34] Anderson, G. P., & Taitt, C. R. EVANESCENT WAVE FIBER OPTIC BIOSENSORS. Optical Biosensors, 83–138, 2008.

[35] Zamarreño, C. R., Rivero, P. J., Hernaez, M., Goicoechea, J., Matías, I. R., & Arregui, F. J. Optical Sensors for Corrosion Monitoring. Intelligent Coatings for Corrosion Control, 603–640 ; 2015.

[36] Bertrand Gauvreau, Alireza Hassani, Majid Fassi Fehri, Andrei Kabashin, Maksim Skorobogatiy, "Photonic bandgap fiber-based Surface Plasmon Resonance sensors," Optic Express, vol. 15, no. 18, pp. 11413-11426, Sep. 2007.

[37]Unser, Sarah; Bruzas, Ian; He, Jie; Sagle, Laura. 2015. "Localized Surface Plasmon Resonance Biosensing: Current Challenges and Approaches" *Sensors* 15, no. 7: 15684-15716.

[38] M. S. Islam, J. Sultana, K. Ahmed, M. R. Islam, A. Dinovitser, B.W.-H.Ng, and D. Abbott, ''A novel approach for spectroscopic chemical identification using photonic crystal fiber in the terahertz regime,'' IEEE Sensors J., vol. 18, no. 2, pp. 575–582, Jan. 2018

[39] M. S. Islam, J. Sultana, A. A. Rifat, A. Dinovitser, B. W.-H. Ng, and D. Abbott, ''Terahertz sensing in a hollow core photonic crystal fiber,'' IEEE Sensors J., vol. 18, no. 10, pp. 4073–4080, May 2018

[40] J. N. Dash and R. Jha, ''Highly sensitive side-polished birefringent PCF based SPR sensor in near IR,'' Plasmonics, vol. 11, no. 6, pp. 1505–1509, 2016

[41] J. N. Dash and R. Das, ''SPR based magnetic-field sensing in microchannelled PCF: A numerical approach,'' J. Opt., vol. 20, no. 11, 2018, Art. no. 115001 67

[42] J. N. Dash, R. Das, and R. Jha, ''AZO coated microchannel incorporated PCF-based SPR sensor: A numerical analysis,'' IEEE Photon. Technol. Lett., vol. 30, no. 11, pp. 1032–1035, Jun. 1, 2018

[43] E. K. Akowuah, T. Gorman, and S. Haxha*, “Design and optimization of a novel surface plasmon resonance biosensor based on Otto configuration,” Journal of Sensors, vol. 17, no. 26, pp. 23511-23521, Dec.2009.

[44] Hyuk Rok Gwon and Seong Hyuk Lee. “Spectral and Angular Responses of Surface Plasmon Resonance Based on the Kretschmann Prism Configuration,” Materials Transactions, vol. 51, no. 6, pp. 1150-1155, Apr.2010.

[45].Chochol, J., Postava, K., Čada, M. *et al.* Experimental demonstration of magnetoplasmon polariton at InSb(InAs)/dielectric interface for terahertz sensor application. *Sci Rep* **7,** 13117 (2017).

[46] M. A. Habib and M. S. Anower, "A Novel Low Loss Porous-Core Photonic Crystal Fiber for Terahertz Wave Transmission," in International Conference on Electrical, Computer and Communication Engineering (ECCE), Cox’s Bazar, Bangladesh, 2017.

[47] M. A. Mollah, A. K. Paul and S. M. A. Razzak “Surface Plasmon Resonance based DualPolarized Photonic Crystal Fiber Refractive Index Sensor,” 2018 Int. Conf. Adv. Electr. Electron. Eng., pp. 1–4, 2018, Gazipur, Bangladesh.

[48] A. A. Rifat et al., “Photonic Crystal Fiber-Based Surface Plasmon Resonance Sensor with Selective Analyte Channels and Graphene-Silver Deposited Core,” Sensors, vol. 15, no. 5 pp. 11499–11510, 2015. 81

[49] R. K. Gangwar and V. K. Singh, “Highly Sensitive Surface Plasmon Resonance Based DShaped Photonic Crystal Fiber Refractive Index Sensor,” Plasmonics, vol. 12, no. 5, pp. 1– 6, 2016.

[50] Hikmat N. Daghestani1 and Billy W. Day2*, “Theory and Applications of Surface Plasmon Resonance, Resonant Mirror, Resonant Waveguide Grating, and Dual Polarization Interferometry Biosensors,” Sensors, vol. 10, pp. 9630-9646, Nov. 2010.

[51] J. Sultana et al., “Dual-Polarized Highly Sensitive Plasmonic Sensor in the Visible to NearIR Dual-polarized highly sensitive plasmonic sensor in the visible to near-IR spectrum,” Optics Express, vol. 26, no. 23, pp. 30347- 30361, 2018.

[52] J. Homola, S. S. Yee, and G. Gauglitz, ‘‘Surface plasmon resonance sensors: Review,’’ Sens. Actuators B, Chem., vol. 54, nos. 1–2, pp. 3–15, 1999.

[53] B. Gupta and R. Verma, "Surface plasmon resonance-based fiber optic sensors: principle, probe designs, and some applications," J. Sens., vol. 2009, 2009.

[54] A. Khaleque and H. T. Hattori, “Ultra-broadband and compact polarization splitter based on gold filled dual-core photonic crystal fiber,” Journal of Applied Physics, vol. 118, no. 14, p. 143101, 2015.

[55]G. A. Lopez, M.-C. Estevez, M. Soler, and L. M. Lechuga, “Recent advances in nanoplasmonic biosensors: applications and lab-on-achip integration,” Nanophotonics 6,123–136 (2017).

[56] R. Otupiri, E. Akowuah, and S. Haxha, “Multi-channel SPR biosensor based on PCF for multi-analyte sensing applications,” Opt. Express 23, 15716–15727 (2015).

[57] M. S. Islam, J. Sultana, A. Dinovitser, K. Ahmed, M. R. Islam, M. Faisal, W.-H. Ng, D. Abbott, “A Novel Zeonex based photonic sensor for alcohol detection in beverages.” IEEE Inter. Conf. on Telecommunications and Photonics (ICTP), pp. 114-18, 2017.

[58] Mohammad Rakibul Islam, Md. Faiyaz Kabir, Khandoker Md. Abu Talha and Md. Saiful Islam, “A novel hollow core terahertz refractometric sensor”, Sensing and Bio-Sensing Research, Volume 25, September 2019, 100295.

[59] Farhana Akter Mou, Md. Moshiur Rahman, Mohammad Rakibul Islam and Mohammed Imamul Hassan Bhuiyan, “Development of a photonic crystal fiber for THz wave guidance and environmental pollutants detection”, Sensing and Bio-Sensing Research, Volume 29, August 2020, 100346

[60] M. R. Islam, A.N.M. Iftekher, F.A. Mou, M.M. Rahman, M.I.H. Bhuiyan, “Design of a Topas-based ultrahigh-sensitive PCF biosensor for blood component detection”, Applied Physics A: Materials Science and Processing, 2021, 127(2), 109

[61] M. R. Islam, M. Mamadou, “Spider web ultrasensitive terahertz photonic crystal fiber for chemical sensing”, Optical Engineering, 2020, 59(8), 087103

[62] S. I. Azzam, M. F. O. Hameed, R. E. A. Shehata, A. M. Heikal and S. S. A. Obayya, “Multichannel photonic crystal fiber surface plasmon resonance based sensor,” Optical and Quantum Electronics, vol. 48, no. 2, pp. 142, 2016

[63] J. Homola, "Present and future of surface plasmon resonance biosensors," Anal. Bioanal. Chem., vol. 377, pp. 528-539, 2003.

[64] A. Rifat, G. Mahdiraji, D. Chow, Y. Shee, R. Ahmed, and F. Adikan, "Photonic Crystal Fiber-Based Surface Plasmon Resonance Sensor with Selective Analyte Channels and Graphene-Silver Deposited Core," Sensors, vol. 15, pp. 11499-11510, 2015

[65]. C. Liu, L. Yang, X. Lu, Q. Liu, F. Wang, J. Lv, T. Sun, H. Mu, and P. K. Chu, “Mid-infrared surface plasmon resonance sensor based on photonic crystal fibers,” Opt. Express, vol. 25, no. 13, pp. 14227–14237, 2017.

[66]. N. Luan, R. Wang, W. Lv, and J. Yao, “Surface plasmon resonance sensor based on D-shaped microstructured optical fiber with hollow core,” Opt. Exp. 23(7), 8576–8582, (2015).

[67]. A. A. Rifat, R. Ahmed, G. A. Mahdiraji and F. R. M. Adikan, “Highly sensitive D-shaped photonic crystal fiber-based plasmonic biosensor in visible to near-IR,” IEEE Sensors Journal 17(9), 2776–2783, (2017).

[68].Q. Xie, Y. Chen, X. Li, Z. Yin, L. Wang, Y. Geng, and X. Hong, “Characteristics of D-shaped photonic crystal fiber surface plasmon resonance sensors with different side-polished lengths,” Appl. Opt. 56(5), 1550–1555, (2017).

[69] G. An, X. Hao, S. Li, X. Yan, and X. Zhang, “D-shaped photonic crystal fiber refractive index sensor based on surface plasmon resonance,” Appl. Opt. 56(24), 6988–6992, (2017).

[70] C. Liu, W. Su, Q. Liu, X. Lu, F. Wang, T. Sun, and P. K. Chu, “Symmetrical dual D-shape photonic crystal fibers for surface plasmon resonance sensing, ” Opt. Exp. 26(7), 9039–9049, (2018).

[71] Islam Md S, Islam MR, Sultana J, Dinovitser A, Ng BW-H, Abbott D. “Exposed-core localized surface plasmon resonance biosensor.” J Optical Soc Am B 2019;36:2306.

[72] Caucheteur C, Guo T, Albert J. “Review of plasmonic fiber optic biochemical sensors: improving the limit of detection.” Anal Bioanal Chem 2015;407:3883–97.

[73] R. Otupiri, E. Akowuah, S. Haxha, H. Ademgil, F. AbdelMalek, A. Aggoun, “A novel birefrigent photonic crystal fibre surface plasmon resonance biosensor,” IEEE Photon. J. 6 (2014).

[74] Y. Zhao, Z.-Q. Deng, and J. Li, “Photonic crystal fiber based surface plasmon resonance chemical sensors,” Sens. Actuators B 202, 557–567 (2014).

[75] Mohammad Rakibul Islam, Md Moinul Islam Khan, Fariha Mehjabin, Jubair Alam Chowdhury, Mohibul Islam, “Design of a fabrication friendly & highly sensitive surface plasmon

resonance-based photonic crystal fiber biosensor, Results in Physics, Volume 19, 2020, 103501, ISSN 2211-3797.

[76] A. Patnaik, K. Senthilnathan, R. Jha, “Graphene-based conducting metal oxide coated D-shaped optical fiber SPR sensor,” IEEE Photon. Technol. Lett. 27 (23) (2015 Aug 25) 2437–2440.

[77] A.K. Paul, A.K. Sarkar, S.A. Razzak, “Graphene coated photonic crystal fiber biosensor based on surface plasmon resonance,” 2017 IEEE Region 10 Humanitarian Technology Conference (R10-HTC), IEEE, 2017 Dec 21, pp. 856–859.

[78] C. Liu, F. Wang, J. Lv, T. Sun, Q. Liu, H. Mu, P.K. Chu, “Design and theoretical analysis of a photonic crystal fiber based on surface plasmon resonance sensing,” J. Nanophoton. 9 (1) (2015 Sep) 093050.

[79] Islam Md S, Sultana J, Ahmmed A Rifat, Ahmed R, Dinovitser A, Ng BW-H, et al. “Dual-polarized highly sensitive plasmonic sensor in the visible to near-IR spectrum.” Opt Express 2018;26:30347.

[80] B. Gauvreau, A. Hassani, M. F. Fehri, A. Kabashin, and M. Skorobogatiy, “Photonic bandgap fiber-based surface plasmon resonance sensors,” Opt. Express, vol. 15, no. 18, pp. 11413_11426, 2007.

[81] J. C. Knight, “Photonic crystal _bers,” Nature, vol. 424, no. 6950, pp. 847_851, Jan. 2003.

[82] Araf Shafkat, “Analysis of a gold coated plasmonic sensor based on a duplex core photonic crystal fiber, Sensing and Bio-Sensing Research,” Volume 28, 2020, 100324, ISSN 2214-1804

[83] M. Rakibul Islam, A. Iftekher, K. Rakibul Hasan, M. Nayen, and S. Bin Islam, "Dualpolarized highly sensitive surface-plasmon-resonance-based chemical and biomolecular sensor," Appl. Opt. 59, 3296-3305 (2020).

[84] V. Kaur, S. Singh, “Design of titanium nitride coated PCF-SPR sensor for liquid sensing applications, Opt. Fiber Technol." 48 (2019 Mar 1) 159–164

[85] Md. saiful islam, Cristiano M. B. Cordeiro, Jakeya Sultana, Rifat Ahmmed Aoni, Shilun Feng, Rajib Ahmed, Mohsen Dorraki, Alex Dinovitser, Brian Wai-him Ng, and Derek Abbott, “A hi-bi ultra-sensitive surface plasmon resonance fiber sensor”, ieee access, digital object identifier 10.1109/access.2019.2922663

[86]D. Li, W. Zhang, H. Liu, J. Hu, and G. Zhou, “High sensitivity refractive index sensor based on multi-coating photonic crystal fiber with surface plasmon resonance at near-infrared wavelength,” IEEE Photon.J. 9, 6801608 (2017).

[87] Alok Kumar Paul,A.K Sarkar, Abdul Khaleque “Twin Core Photonic Crystal Fiber Plasmonic Refractive Index Sensor”, IEEE Sensors Journal (Volume: 18, Issue:14, July15, 15 2018)

[88]A. A. Rifat, F. Haider, R. Ahmed, G. A. Mahdiraji, F. R. M. Adikan, and A. E. Miroshnichenko, “Highly sensitive selectively coated photonic crystal fiber-based plasmonic sensor,” Opt. Lett. 43, 891–894 (2018).

[89]M.F.O. Hameed, Y.K. Alrayk, A.A. Shaalan, W.S. El Deeb, S.S. Obayya, “Design of highly sensitive multichannel bimetallic photonic crystal fiber biosensor,” J. Nanophotonics, vol. 10, pp. 046016–04601, 2016.

[90]T. Huang, “Highly sensitive SPR sensor based on D-shaped photonic crystal fiber coated with indium tin oxide at near-infrared wavelength,” Plasmonics vol. 12, pp. 583–588, 2017.